Quaternary Science Reviews 385 (2026) 110007

Contents lists available at ScienceDirect

Quaternary Science Reviews

journal homepage: www.elsevier.com/locate/quascirev

# Holocene hydroclimatic variability and Neolithic to the Bronze Age human dynamics recorded in Grotta Battifratta cave (Rieti, central Italy)

L. Forti [a,*], S. Costanzo [a], S. Milli [b,c], D. Tentori [c], I. Mazzini [c], P. Lotti [a], A. Proietto [a], A. Mancini [b], E. Regattieri [d], D. Moscone [e], E. Carletti [f], E. Chiarabba [f], M. Mulargia [g], N. Marconi [f], A. Zerboni [a], C. Conati Barbaro [f]

[a] Dipartimento di Scienze della Terra "Ardito Desio", Università di Milano, Milano, Italy
[b] Dipartimento di Scienze della Terra, SAPIENZA Università di Roma, Roma, Italy
[c] CNR - Istituto di Geologia Ambientale e Geoingegneria, Montelibretti, (RM), Italy
[d] CNR - Istituto di Geoscienze e Georisorse, Pisa, Italy
[e] Institute of Pre- and Protohistoric Archaeology, Christian-Albrechts-Universität zu Kiel, Kiel, Germany
[f] Dipartimento di Scienze dell'Antichità, SAPIENZA Università di Roma, Roma, Italy
[g] Dipartimento di Storia, Scienze dell'Uomo e della Formazione, Università di Sassari, Sassari, Italy

ARTICLE INFO

*Keywords:*
Grotta Battifratta
Cave geoarchaeology
Holocene hydroclimate
Karst environment
y
Neolithic–Bronze age
Central Italy
Apennines

ABSTRACT

Grotta Battifratta cave is a key archaeological cave located along a travertine escarpment in the Farfa Valley (Rieti, central Italy), within the middle Tiber catchment. Recent interdisciplinary investigations by Sapienza University of Rome have documented a well-preserved stratigraphic succession spanning from the Middle Palaeolithic to the post-Medieval period, with particularly detailed evidence for Neolithic and Bronze Age activity at the cave entrance. This study integrates archaeological excavation with sedimentological, micromorphological, geochemical, mineralogical, micropalaeontological and radiocarbon analyses to reconstruct the Holocene cave infill and its links to human use. Neolithic deposits (end of the 6$^{th}$–beginning of the 5$^{th}$ millennium BCE) accumulated through short-lived depositional and erosional events driven by alternating slope stability, surface runoff and episodic karst reactivation. Bronze Age evidence is more spatially restricted and reflects episodic use, likely linked to pastoral practices, during a phase of hydrological reorganisation of the karst system followed by low-energy carbonate sedimentation. Post-Medieval ceramics in the uppermost deposits provide a terminus post quem for final infilling, which falls within the Little Ice Age phase of hydroclimatic instability. Overall, Grotta Battifratta cave shows how Holocene cave deposits record the intertwined effects of environmental processes and human activities, providing a geoarchaeological archive of human-karst landscape interactions in inland central Italy.

## 1. Introduction

Caves are widely recognized as archives of natural and anthropogenic processes, offering reliable insights into long-term environmental change and human occupation (White, 1988; Farrand, 2001; Cremaschi et al., 2005, 2014; Goldberg and Sherwood, 2006; Ford and Williams, 2007). Owing to their relatively stable microclimates and sheltered conditions, which favour the preservation of stratified deposits despite intense outside weathering, caves have significantly advanced our understanding of past climatic fluctuations, depositional processes, and cultural practices throughout the Quaternary, enabling reconstructions of socio-environmental dynamics from the Palaeolithic onwards (Goldberg and Sherwood, 2006; Angelucci et al., 2009; Cremaschi et al., 2014; Mallol and Goldberg, 2017; Spinapolice et al., 2022). Their sedimentary successions, spanning from the daylight zone to deeper chambers, can capture subtle traces of past human behaviours and environmental transformations (Hunt et al., 2015; Goldberg and Sherwood, 2006).

Caves function as major sedimentary traps within karst landscapes. Sediment sources are highly diverse and include products of bedrock physical weathering, such as flaking, spalling, exfoliation, and granular disintegration, together with colluvial and alluvial inputs transported

* Corresponding author.
*E-mail address:* luca.forti@unimi.it (L. Forti).

https://doi.org/10.1016/j.quascirev.2026.110007
Received 22 December 2025; Received in revised form 15 April 2026; Accepted 17 April 2026
Available online 28 April 2026

from outside the cave and along the karst network, as well as aeolian material, biogenic accumulations, and anthropogenic debris (Goldberg and Sherwood, 2006; Carroll, 2012; Hall et al., 2012; Karkanas et al., 2021; Zerboni et al., 2022). As a consequence, archaeological cave studies have long represented a key domain for geoarchaeological research, integrating sedimentology, micromorphology, geochemistry, and, more recently, molecular approaches to disentangle site formation processes, refine chronologies, and assess the nature and intensity of human presence within dynamically evolving depositional environments (Farrand, 2001; Cremaschi et al., 2005, 2014; Ghinassi et al., 2009; Nicosia and Stoops, 2017; Massilani et al., 2022; Morley et al., 2023; Aldeias and Stahlschmidt, 2024; Costanzo et al., 2024). In this framework, geoarchaeological analyses have proven essential for distinguishing geogenic deposits from anthropogenic components, including combustion residues and stabling-related accumulations, thereby allowing a more precise reconstruction of depositional processes and activity patterns within cave environments (Angelucci et al., 2009). This methodological refinement has substantially improved our understanding of how caves were used over time, their role within foraging and pastoral systems, and the ways in which these functions responded to climatic variability and cultural change.

Recent decades have seen a marked growth of cave-based geoarchaeological research across the Mediterranean and Europe. In this wider framework, Italian karst systems offer multiple stratified sequences from the Palaeolithic to the Bronze Age (Cremaschi and Ferraro, 2007; Rellini et al., 2013, 2020; Boschian et al., 2017; Angelucci et al., 2019; Moroni et al., 2019; Cremaschi et al., 2005, 2022, 2026; Pieruccini et al., 2022; Spinapolice et al., 2022; Ryan et al., 2024).

Applications of geoarchaeological approaches to cave contexts in peninsular Italy have highlighted the complexity of Holocene infill sequences, where anthropogenic inputs such as combustion residues, dung accumulations and trampled surfaces alternate with slope-derived sediments and water-lain deposits (Boschian et al., 2017; Cremaschi et al., 2020, 2026).

These stratified archives have proven particularly valuable for reconstructing land-use dynamics and for clarifying the interaction between natural processes and cultural activity in karst environments, contributing to broader reconstructions of paleoenvironmental change, site formation dynamics, and human behaviour in Holocene Mediterranean landscapes (Cremaschi et al., 2005, 2020, 2026 ; Cremaschi and

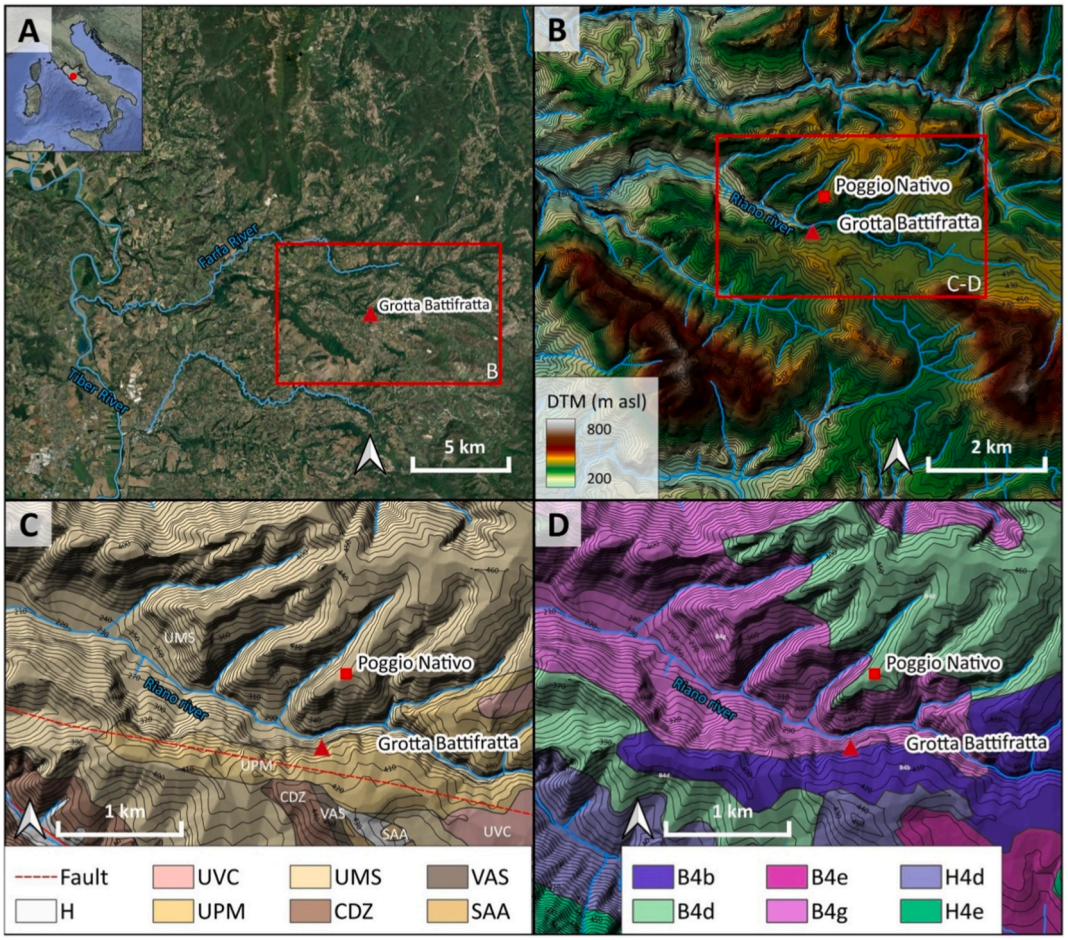


**Fig. 1.** A) Google Earth imagery of the study area with the location of the Grotta Battifratta (42.209876 N, 12.792541 E). B) DTM of the area surrounding Grotta Battifratta (DTM elaborated in QGIS 3.34; freely downloaded from https://tinitaly.pi.ingv.it/; Tarquini et al., 2023). C) Geological map of the area in which the main geological formations are reported (H, Holocene deposits; UVC, Castelnuovo di Farfa Syntem; UPM, Poggio Moiano Syntem; UMS, Monteleone Sabino Synthem; CDZ, Scaglia Cinerea Detritica Fm.; VAS, Scaglia Variegata Fm.; SAA, Scaglia Rossa Fm.) (modified from Servizio Geologico d'Italia, 2009; sheet 357 Cittaducale). D) Pedological map of the study area, in which are reported the main pedological features (modified from Carta dei Suoli del Lazio). In detail, B4b refers to terraces and transitional slopes on travertine and reworked volcanic deposits, with Haplic Luvisols and Calcaric Cambisols. B4d indicates slopes on gravel and marine sands, featuring Endoskeletic Cambic Calcisols. B4e includes slopes and summit areas on cemented sandy gravel, with Endoskeletic Cambic Calcisols, Calcaric Skeletic Epileptic Phaeozems, and Calcaric Cambisols. B4g covers slopes on sandy gravel, with Calcaric Skeletic Epileptic Phaeozems, Calcaric Cambisols, and Calcaric Regosols. H4d describes hillsides on limestone–marl alternations (6–35% slope), with Calcaric Epileptic Regosols, Calcaric Skeletic Epileptic Cambisols, and Calcaric Regosols. H4e refers to hillsides on limestone–marl alternations (>35% slope), with Rendzic Leptosols, Endoskeletic Cambic Endoleptic Phaeozems, and Epileptic Rendzic Phaeozems.

Ferraro, 2007; Iaconis and Boschian, 2008; Boschian et al., 2017; Rellini et al., 2020)

Within this Mediterranean cave framework, the present research focuses on Grotta Battifratta (Rieti, central Italy), where a wide and cross-disciplinary geoarchaeological approach is employed to investigate the Holocene sedimentary infilling in relation to climatic variability, karst hydrology, and human land use. By integrating archaeological data with sedimentological, micromorphological, geochemical, mineralogical and micropaleontological analyses, we reconstruct the processes controlling sediment accumulation and preservation and evaluates their implications for human occupation from an understudied inland sector between the central Apennines and the Tiber Valley.

## 2. Study area: geology, soils and climate

Grotta Battifratta cave (42.209876° N, 12.792541° E, 370 m asl) is a travertine cave system located approximately 40 km northeast of Rome, within the municipality of Poggio Nativo (Rieti), in the southern foothills of the Sabina Mountains, which are part of the central Apennine fold-and-thrust belt that primarily developed during the Neogene (Fig. 1A and B). The local bedrock complex surrounding the cave is composed of the Mesozoic to Cenozoic sedimentary succession belonging to the Umbria–Marche–Sabina shelf-to-pelagic domain that is overlain by Plio-Pleistocene continental deposits (Servizio Geologico d'Italia, 2009; Cosentino et al., 2010). Specifically, the lithostratigraphic succession comprises Upper Cretaceous to Lower Eocene reddish marly limestones with chert (SAA), Paleocene to Lower Eocene marls and bioclastic marly limestones, and Middle Eocene marly limestones and marls intercalated with violet to black chert (VAS and CDZ), overlain by the Plio-Pleistocene succession. This includes conglomerates and sandy–silty layers (UMS), calcareous tufas and travertines (UPM) (hosting Grotta Battifratta and other caves and rockshelters), medium-to fine--grained sands, and, at the top, Holocene slope, fluvial, and colluvial deposits with local levels of volcanic deposits (H) (Fig. 1C). The pedological cover in the study area reflects diverse soil-forming processes shaped by variations in parent material and topography. The maps soil units B4b, B4d, B4e, B4g, H4d, and H4e (Fig. 1D), representing distinct litho-topographic associations, each supporting specific soil types classified according to the World Reference Base (WRB, 2015) and documented in the Carta dei Suoli del Lazio (1:250,000 scale) (Napoli et al., 2019). Overall, soils of the area display coherent degrees of alteration of the marly/limestone and travertine bedrocks, with catenas of regosols, cambisols, luvisols, and phaeozems forming according to lateral changes in slope, substrate texture, substrate compaction, and arboreal cover.

The present-day climate experiences a Mediterranean to sub-Mediterranean regime with strong precipitation seasonality: rainfall is concentrated in autumn–winter, whereas summer is comparatively dry (WMO, 2017; ISPRA, 2022). Mean annual precipitation falls in the 700–1000 mm class in the main valley/foothill areas and increases to 1000–1500 mm across the Monti Sabini ridge, while annual temperatures are around 12–14 °C (Tmean) with ~18–20 °C (Tmax) and ~6–8 °C (Tmin), implying a marked thermal range inland. This seasonal contrast links directly to geomorphic responses: summer drought favours fuel drying and fire susceptibility, and the first intense autumn rains promote event runoff and slope erosion when ground cover is reduced (ISPRA, 2022). Present land cover is a mosaic of agricultural patches (including permanent crops) and extensive broad-leaved/mixed forests; vegetation belts are dominated by thermophilus deciduous oak forests (e.g., *Quercus pubescens* s.l., *Q. cerris*, locally *Q. frainetto*), with chestnut and beech at higher elevations (Biondi et al., 2014; Bottacci and Clauser, 2022).

## 3. The karst system of Grotta Battifratta

Grotta Battifratta opens on the left slope of the Riano Valley, a tributary of the Farfa River in the Tiber River basin (Fig. 1A). The karst system develops within Middle Pleistocene travertine deposits of the Poggio Moiano Synthem (UPM), dated to >350 ka (Manfra et al., 1976; Servizio Geologico d'Italia, 2009; Cosentino et al., 2010) (Fig. 1C). The UPM consists of encrusting limestones and bioinduced lacustrine limestones formed by calcium carbonate precipitation from flowing waters over vegetated substrates. Surrounding the cave, laminated to thin-bedded, non-cemented brownish limestones composed of calcareous silt or silty sand are Interbedded with travertines, and likely represent palaeosols or sediments deposited in flooded depressions or small ponds.

Grotta Battifratta is an epigenic karst system (*sensu* De Waele and Gutiérrez, 2022) with a wide cave entrance, transitioning through a narrow cave mouth into an internal conduit network developed along fractures and bedding planes in the travertine (Figs. 2 and 3). The cave entrance, originally a cave chamber exposed by slope retreat, is marked by a remnant stalactite (Fig. 3), and measures 18 m in width, 8.5 m in depth, and 6 m in height. Its size and shape are controlled by structural discontinuities and further modified by mechanical collapse (e.g., freeze-thaw cycles) and biological processes (e.g., root etching, micro-pitting). In earlier phases, the area likely functioned as a cave mouth, influenced by a spring discharge point that periodically reworked the deposits via floodwaters. The internal cave system displays a linear to angular, eastward-oriented cave profile, with a large chamber filled with silty-clay sediments and speleothems linked to recharge zones (Fig. 3). The main conduit (~60 m long) exhibits keyhole morphology, with an upper rounded phreatic tube entrenched by a vadose canyon, infilled with reddish-brown clays and collapse debris (Fig. 3). This dual morphology indicates hydrological shifts from phreatic to vadose conditions, related to discharge variations and water table lowering due to climatic changes (Ford and Williams, 2007; De Waele and Gutiérrez, 2022). The cave alternated periods of active and passive hydrological phases (Woodward and Goldberg, 2001). During active phases, high-energy conduit flows transported coarse, organic-rich sediments. In passive phases, autogenic recharge through the epikarst, slow percolation, seasonal dripwater, and local ponding favoured the winnowing of silts and clays, often with illuvial features (Sasowsky and Mylroie, 2007).

Morphological variations (e.g., constrictions, bends, roughness) and sedimentation influenced flow velocity and hydraulic gradient, producing sedimentary facies with marked lateral and longitudinal variability. Major recharge events can erode earlier deposits and redistribute sediment along the karst system, whereas quieter phases favour the settling of fine-grained material in ponded areas and the development of illuvial features driven by slow percolation and seasonal dripwater. (Ford and Williams, 2007; De Waele and Gutiérrez, 2022).

## 4. Archaeological background

Archaeological evidence for the earliest phases of human occupation in the Sabina mountain area remains fragmentary, despite its central position within the network of routes connecting the Tiber Valley, the Central Apennines and further east, the Sibillini Mountains and the Adriatic coast. Nevertheless, the available record, primarily from surface survey and sporadic excavations, documents long-term human presence spanning Prehistory and Protohistory (Acanfora, 1962; Albertini et al., 2019; Bulgarelli, 1979;Guidi and Santoro, 2012; Filippi and Pacciarelli, 1991; Rolfo et al., 2016). Within this framework, the Farfa Valley and its tributaries stand out for the concentration of caves and rock shelters with a high archaeological and paleoenvironmental potential (Conati Barbaro et al., 2024a).

Grotta Battifratta (Poggio Nativo, Rieti) was first investigated in the 1980s, when exploratory soundings carried out by the Italian Institute of Human Palaeontology identified two principal occupation phases at the cave entrance, attributed to the Neolithic and the Bronze Age (Segre Naldini and Biddittu, 1985, 1988). Middle Bronze Age (MBA) pottery,

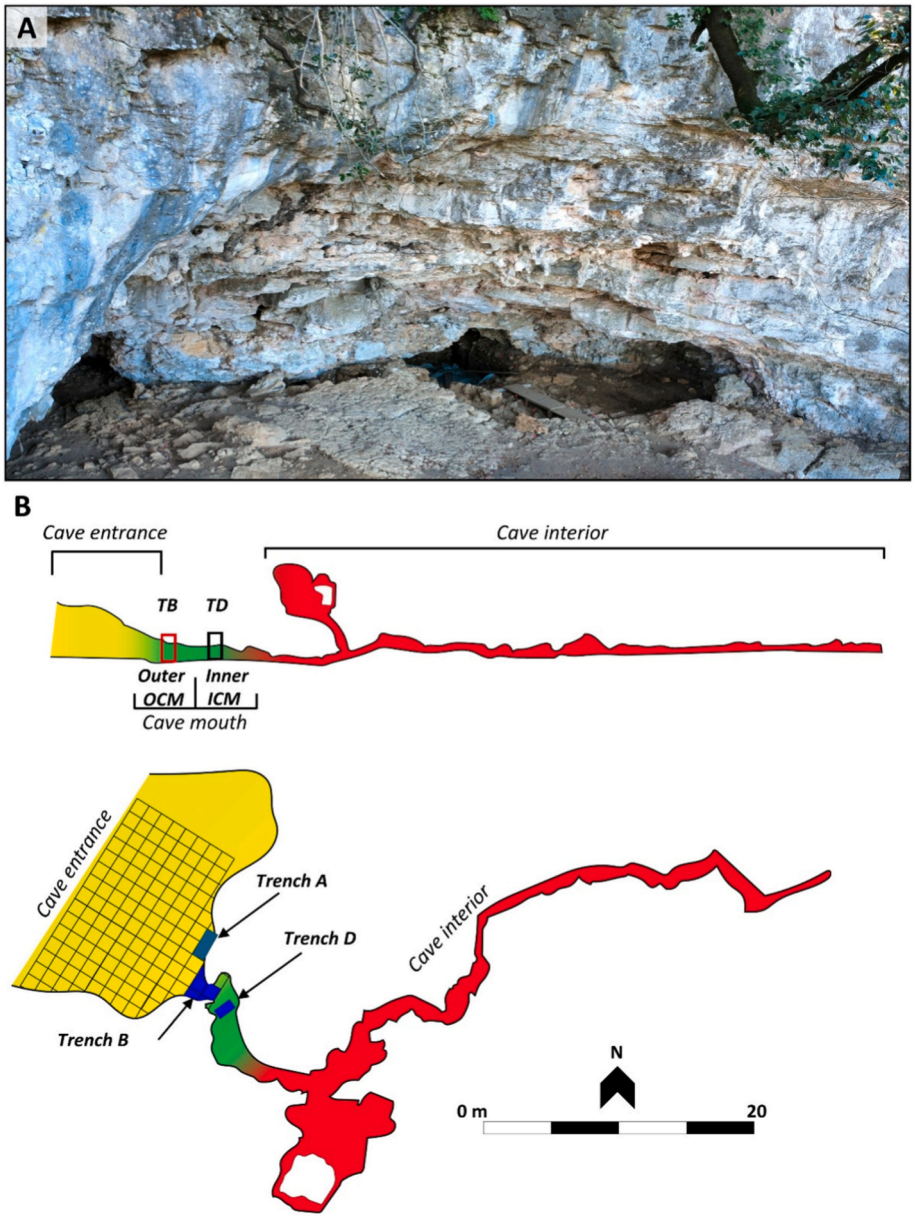


**Fig. 2.** A) UAV acquisition of the cave entrance of Grotta Battifratta and the travertine escarpment. B) Plan and profile cave survey (modified from the cave survey made by the Gruppo Speleo Archeologico Vespertilio) with the position of different sectors of the cave. The blue and light blue colour are the main archaeological excavation areas.

associated with scattered human remains in the inner corridor, suggested funerary use during this phase (Segre Naldini and Biddittu, 1985).

Archaeological investigations resumed in 2021 within the *Farfa Valley Project. Caves, People, and Past Environments*, directed by Department of Antiquity Sciences at Sapienza University of Rome (Conati Barbaro et al., 2024a). Excavations focused on the cave entrance and the adjacent internal sectors, exposing a long stratigraphic sequence spanning from the late Pleistocene to the early modern period (Figs. 4 and 5). This investigation has documented an older phase of occupation at the cave entrance (Trench A) dating to the Upper Pleistocene (Fig. 2). This as indicated by a lithic assemblage employing the *Levallois* technique, in association with faunal remains, including large mammal bones such as *Bos primigenius* (Conati Barbaro et al., 2024a).

Trench B (TB), located at the cave mouth, yielded a Neolithic stratigraphic succession where the material recovered is homogeneous and consistent with the radiocarbon dates obtained so far (see Table 3 in § 6.4), thereby allowing the occupation of the site to be securely placed within a relatively short chronological span of a few centuries. The use of the cave seems to be closely linked to the presence of a seasonal water source.

The pottery assemblage includes vessels and decorative motifs characteristic of both the central Adriatic (Ripoli-style and Catignano cultures) and Tyrrhenian areas (Incised-lines ware). The presence of a Fiorano-style mug decorated with incised motifs further suggests cultural interactions extending to the Po Plain. Moreover, the predominance of closed shapes such as mugs, carinated vases, and jars indicates a functional emphasis on water-related activities (Conati Barbaro et al. 2024a, 2024b) (Fig. 5).

The lithic assemblage is characterized by a substantial presence of bladelets, cores, and other elements linked to the laminar *chaîne opératoire*, indicating that knapping activities took place on-site. The use of high-quality raw materials, especially fine-grained chert obtained from both primary and secondary deposits (Carletti et al., 2026), points

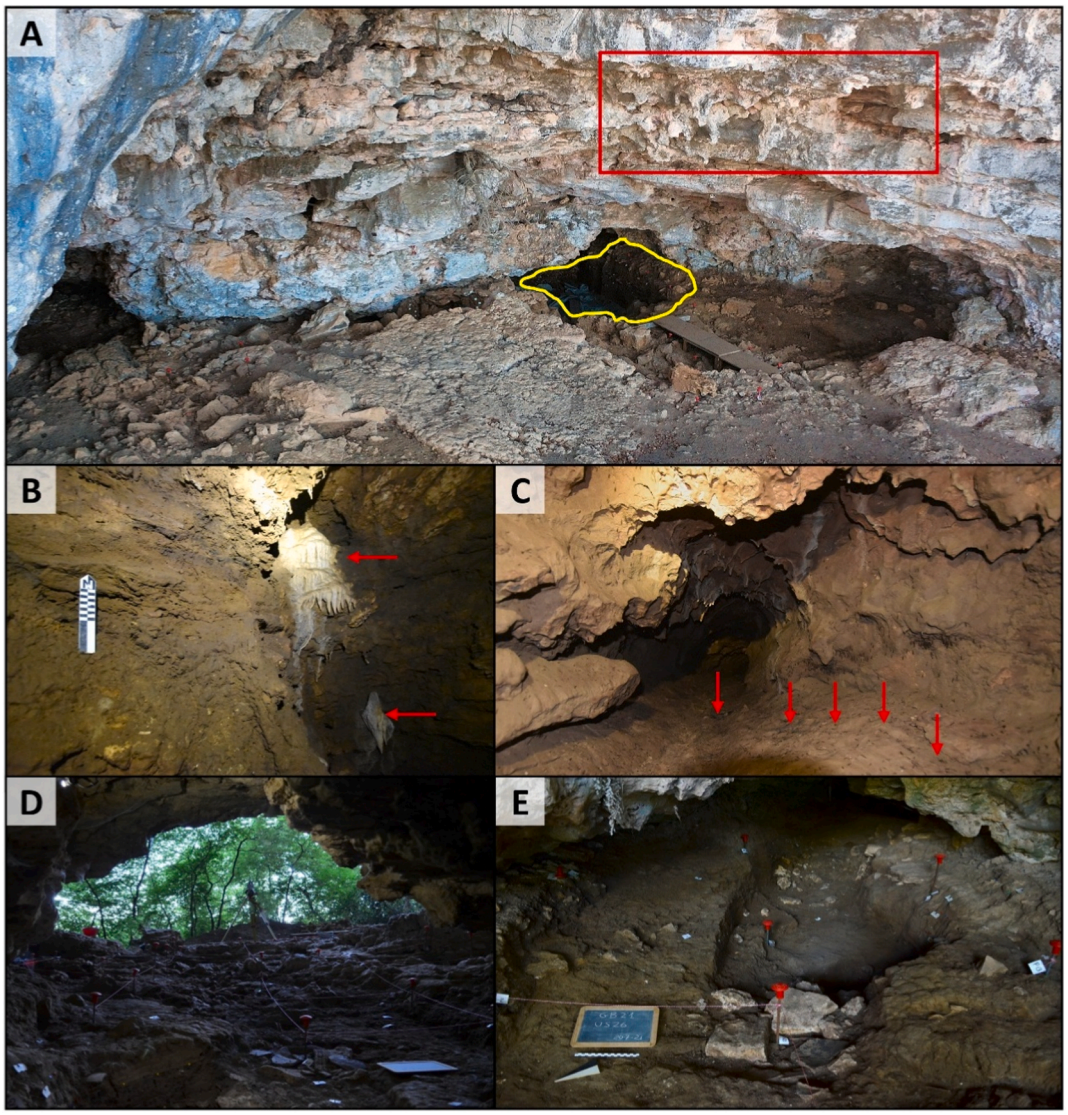


**Fig. 3.** A) Field picture of the cave entrance of Grotta Battifratta. Red polygon indicates remnant fossil stalagmites and the yellow polygon the outer sector of the cave mouth (TB); B) Detail of the inner chamber area filled with fine sediments, with speleothems visible in the background (red arrows). C) Detail of the conduit area and fine sediments (red arrows). D-E) The outer sector of the cave mouth (Trench B).

to diverse procurement strategies involving both local and non-local sources (Carletti et al., 2025a, 2025b) (Fig. 5).

The discovery of well-preserved, partially articulated human remains of a nonadult (SU45) and of an adult male (SU71/SU60) (Thompson, 2024), in two overlapping stratigraphic units, suggests that the cave was also used as a burial site. A clay figurine, a bone pendant, and a fragmented stone bracelet found in proximity to the nonadult's remains; however, their primary association as burial offerings remains tentative, as the stratigraphic context appears to have been disturbed by post depositional water-flow alterations (Conati Barbaro et al., 2025) (Fig. 5).

Human occupation of the cave appears to have ceased at the beginning of the 5th millennium BCE, with no evidence of subsequent activity until the Bronze Age, between the 18th and 14th centuries BCE. During this period, Middle Bronze Age (MBA) groups reoccupied the site, utilizing the inner part of the cave as a funerary space. In contrast, the area near the cave entrance likely served domestic or pastoral functions, such as the sheltering of livestock or food preparation, suggested by the presence of a combustion feature.

Segre Naldini and Biddittu (1985) reported the presence of scattered human remains in association with MBA 3 ceramics within the internal corridor, confirming the cave's use for burial during this phase. The ceramic assemblage is dominated by jars, mugs, and carinated bowls, decorated primarily with incised or excised geometric motifs such as meanders and zigzags filled with dots, often enhanced with white inlay. These decorative features are typical of MBA 3 contexts in central Italy.

During the Bronze Age, the cave may have been used by pastoral communities moving through the Riano River Valley along seasonal transhumance routes, with Grotta Battifratta serving as one of several temporary stopovers along their journey to or from the Apennines. During this phase, MBA groups reoccupied the site, utilizing the inner part of the cave as a funerary space (Segre Naldini and Biddittu, 1985). In contrast, the area near the cave entrance likely served domestic or pastoral functions, such as the sheltering of livestock or food preparation, suggested by the presence of a combustion feature excavated in the cave mouth area (Conati Barbaro et al., 2024a) (Fig. 4).

The most recent occupation is documented by a maiolica jug found at the top of the sequence, dated to the first half of the sixteenth century CE and comparable to material from the Crypta Balbi in Rome (Conati Barbaro et al., 2024a) (Fig. 5).

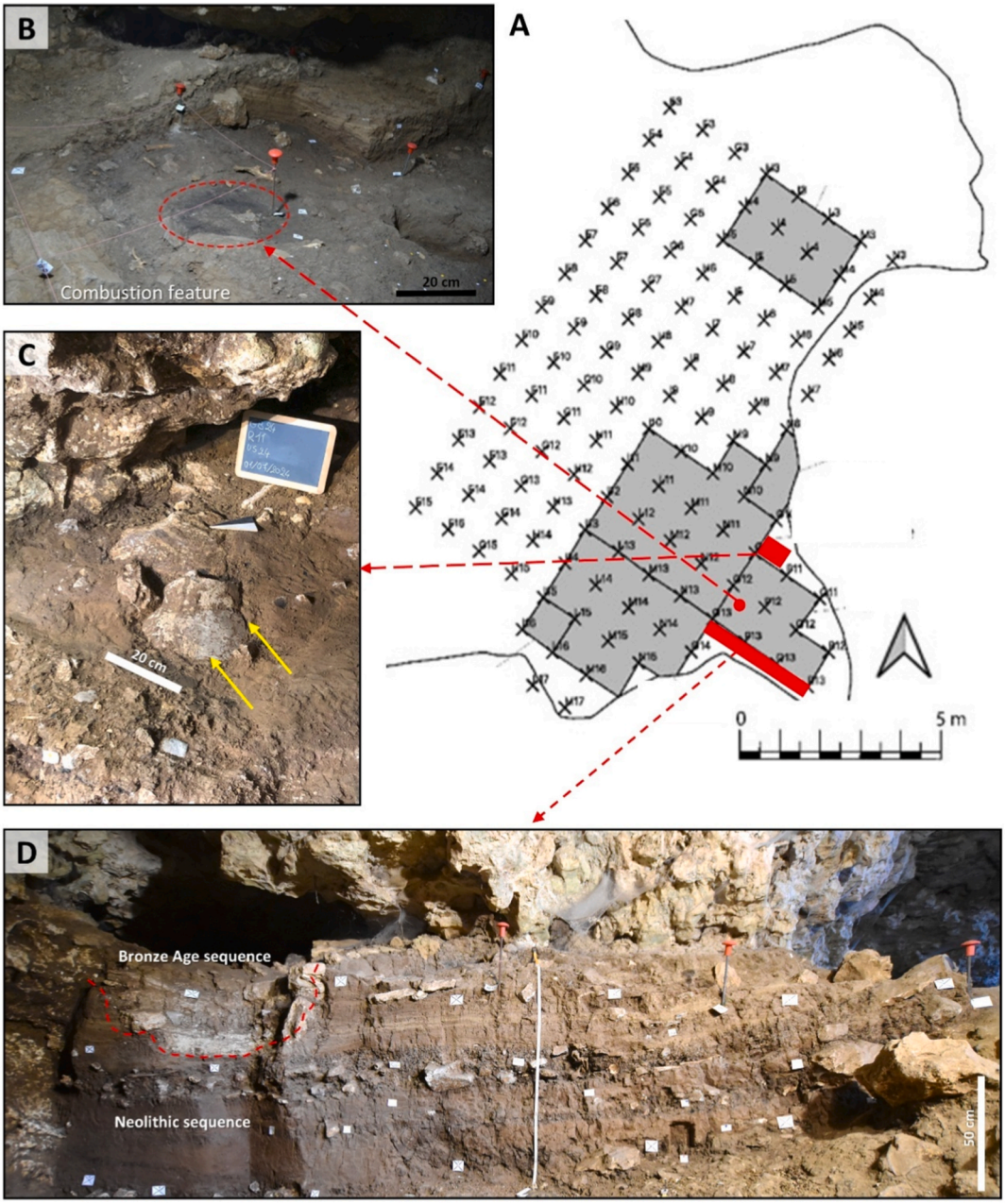


**Fig. 4.** A) Excavation areas located in proximity to the cave entrance and cave mouth at Grotta Battifratta (see also Fig. 2). B) Detail and orthophoto of the main combustion feature (Bronze Age) identified highlighted by red dashed outlines. C) Detail of the excavation area at the cave mouth showing the exposure of Neolithic pottery fragments visible on the surface (yellow arrows. D) Final stratigraphic section (TB) at the cave mouth showing the Neolithic deposits overlain by Bronze Age. The dashed red line marks the boundary between the Bronze Age deposits and the underlying Neolithic sequence.

## 5. Materials and methods

Our study investigates the cave mouth area, which preserves evidence of Neolithic and Bronze Age occupations. For analytical purposes, the cave mouth was subdivided into two sectors: the Outer Cave Mouth (OCM) and the Inner Cave Mouth (ICM) (Figs. 2 and 3). The OCM corresponds to the portion of the cave closest to the dripline and is therefore more directly influenced by external agents such as rainfall, temperature fluctuations, and sedimentary inputs from slope wash or surface runoff. The OCM sector was investigated through the archaeological excavation of Trench B (TB).

The ICM, by contrast, lies further inside the cavity and is less affected by these exogenous processes, representing a more sheltered environment where depositional dynamics are modulated by internal cave conditions and attenuated external influences. The ICM sector was investigated through the excavation of Trench D (TD). The stratigraphic investigation of the archaeological cave deposits at Grotta Battifratta focused on TB and TD, which were systematically sampled for a range of laboratory analyses.

Sediment samples for grain-size analysis, and for the measurements of organic and inorganic carbon content and X-ray diffraction (XRD) were collected at 10 cm intervals, as these analyses required larger amounts of material and provided a broader resolution characterization of the exposed sedimentary succession. In contrast, samples for micropalaeontological analysis (ostracods) and were collect at 5 cm intervals to obtain higher-resolution insights into the microenvironmental changes. In addition, undisturbed blocks for thin-section micromorphology were extracted from selected stratigraphic units, and selected


**Fig. 5.** A-D) Neolithic materials: A, Painted Ripoli- style vase (scale bar 5 cm); B, polished stone ring (scale bar 2 cm; B, tools, débitage elements, core (scale bar 5 cm); D, clay figurine (scale bar 1 cm). E-F) Bronze Age pottery (scale bar 2 cm for E and 5 cm for F). G) 16$^{th}$ century CE glazed maiolica jug (scale bar 2 cm).

samples for provenance analysis were collected from both the TB and TD sections. A total of seven samples for radiocarbon dating were obtained from sections TB and TD.

### 5.1. Stratigraphy, sedimentology and geochronology

Archaeological excavation was carried out according to stratigraphic units (SUs) in both TB and TD.

Each SU was field described in detail and assigned a colour using the Munsell Soil Colour Chart (Munsell Color Company, 1994). Stratigraphic profiles in both TB and TD were subdivided based on distinct pedo-sedimentary characteristics. Major erosional surfaces within both profiles were also identified. Subsequent sampling was performed for sedimentological analysis, with samples collected at 10 cm intervals or according to SU thickness and interfaces. 12 samples were analysed from section TB and 9 from section TD. Grain-size (GS) analyses were conducted using the laser diffraction technique to determine Particle Size Distribution (PSD) (Eshel et al., 2004).

Seven samples from TB and TD were selected for AMS-radiocarbon dating and were sent to the Dating and Diagnostic Center (CEDAD) of Salento University (Italy). Radiocarbon dates were calibrated with OxCal (https://c14.arch.ox.ac.uk/oxcal.html) using the IntCal20 calibration curve (Reimer et al., 2020) (see Table 3), and the archaeological chronology was established with reference to the regional framework proposed by Palmisano et al. (2021).

### 5.2. Geochemical and mineralogical analysis

Organic and inorganic carbon contents were analysed on 38 samples collected at 5 cm intervals, both TB and TD, to obtain high-resolution data on Total Carbon (TC), Total Organic Carbon (TOC), and Total Inorganic Carbon (TIC). Samples were oven-dried (~50 °C), disaggregated manually, and sieved to retain the <2 mm fraction. This was then ground into powder for analysis.

TC was measured by weighing aliquots in tin capsules to six decimal places and combusting them in a Thermo Fisher Flash 2000 Elemental Analyzer. Gases were separated and quantified by thermal conductivity, yielding TC values in weight percent. TOC was determined on carbonate-bearing samples after pre-treatment with 18% HCl to remove inorganic carbon. Powdered samples were acidified in silver capsules until effervescence stopped, dried at 65 °C, sealed, and analysed. TIC was obtained by subtracting TOC from TC.

For XRD analysis, 19 representative samples from trenches TB and TD were powdered with an agate mortar. Powders were packed into standard holders (Bragg–Brentano geometry) using the backfilling technique to minimise preferred orientation. X-ray diffraction was

performed using a Panalytical X'Pert Pro diffractometer (Cu-Kα, λ = 1.5406 Å; 40 kV, 40 mA), scanning from 5° to 70° 2θ, with 0.033° steps and 0.5 s/step. Mineral phases were identified using Panalytical X'Pert HighScore software (Degen et al., 2014) by comparison with reference patterns from the internal database.

### 5.3. Thin section micromorphology

A total of 10 undisturbed sediment blocks were collected for micromorphological analysis: four from TB, five from TD, and one from a Bronze Age combustion feature (see § 4). Sampling was carried out on freshly cleaned stratigraphic profiles using standard procedures to preserve the internal structure and minimise disturbance. Attention was paid to maintaining the original orientation and integrity of each block, which were carefully wrapped and stabilised for transport.

Thin section preparation was performed by the laboratory Massimo Sbrana, Servizi per la Geologia (Piombino, Italy), following the protocol described by Murphy (1986). Samples were air-dried, impregnated with polyester resin under vacuum, sliced, mounted on glass slides, and polished to 30 μm-thick sections measuring 55 × 95 mm.

Micromorphological observations were conducted using an Olympus BX41 microscope equipped with 2x, 4x, 10x, and 40x magnifications and an Olympus E420 digital camera for documentation; observations were performed under plain polarized light (PPL) and cross-polarized light (XPL). Descriptions followed the terminology and classification criteria of Stoops (2021), with interpretative support from reference works and illustrated atlases including Nicosia and Stoops (2017), Macphail and Goldberg (2018), and Stoops et al. (2018).

### 5.4. Compositional analysis

Samples from TB (TB40 and TB50) and from TD (TD40, TD50, and TD70) sections were selected for compositional analysis. Sand samples were dry-sieved to isolate the 125–500 μm fraction, chosen to represent the typical grain-size range of the studied deposits and to provide a dataset complementary to the micromorphological observations. The selected fractions were impregnated with resin and prepared as polished thin sections for petrographic analysis.

Framework grain composition for samples TB40, TB50 and TD70 was determined following the Gazzi-Dickinson point-counting method (Ingersoll et al., 1984), in which each grain is classified according to its mineralogical identity at the scale of individual crystal fragments. Counted grains were grouped into monomineralic and polymineralic categories. Raw proportions were calculated based on total counts, and percentages were recalculated to 100% to obtain standardized compositional parameters, including QFL (quartz–feldspar–lithic) proportions, QmKP (monocrystalline quartz–feldspar relationships), and LmLvLs (volcanic–sedimentary lithic subpopulations).

### 5.5. Ostracod analysis

A total of 37 samples from TB and TD were processed for micropaleontological analysis. Each sample was soaked in a 5% $H_2O_2$ solution for 24 to 48 h to disaggregate the sediment, then wet-sieved using a 0.063 mm mesh and air-dried. The dried residues were hand-picked to collect both juvenile and adult ostracod valves. Identification of adult ostracod valves and other biological remains was conducted under a stereomicroscope and supplemented by Scanning Electron Microscope (SEM) imaging. Abundant and well-preserved ostracods were recovered from only four samples, including both adult and juvenile forms. The approximate juvenile-to-adult ratio of 8:1 suggests *in situ* assemblages (following Whatley, 1988; Boomer et al., 2003). The presence of very early-stage moults further indicates a low-energy depositional environment.

## 6. Results

### 6.1. Field description of the outer cave mouth section TB and the inner cave mouth section TD

Excavation of the outer cave mouth sector revealed a shallow north–south-aligned depression, approximately 4 m in length and between 0.5 m and 2 m in depth, at the base of the Neolithic sequence.

It is bounded to the west by a ramp of roof-fall blocks that isolates it from the adjacent cave entrance. Repeated collapse events created a natural sediment trap, preserving a stratified archaeological sequence dated to the Neolithic, Bronze Age, and historical period.

Three stratigraphic sections (TB-North, TB-South, and TB-East) were cleaned and sampled during the excavation. Despite general lateral consistency, minor intra-unit variations reflect local topography, roof-fall clasts, and human disturbance. TB-South (in the previous chapters, TB) was selected as the main reference profile (Fig. SI 1).

TB reveals a vertically continuous succession of fine-grained cave sediments, subdivided into eight stratigraphic units (from top to bottom SUs 12-25-26-24-44-45-57-60), each marked by distinct pedo-sedimentological properties and archaeological features.

The SUs 12-25-26 are the uppermost part of the sequence, consisting of cross-laminated sand, sandy silt, and silty clay, showing evidence of erosive surfaces, roof-fall blocks, and a fining-upward trend (Fig. 6). From SU 24 downwards, the TB shows much evidence of anthropogenic influence. SU 24 and SU 45 are rich in charcoal, faunal remains, and pottery sherds with some evidence of preferential orientation. SU 44, by contrast, is archaeologically poor, featuring voids with clay illuviation and manganese coatings. Lower units (SU 57-60) include silty sand to clay-rich sediments, often with dispersed charcoal, carbonate concretions, and travertine clasts (Fig. 6).

In the inner cave mouth sector, trench TD (in the previous chapters, TD) was excavated to expose the stratigraphic sequences of the internal corridor, which was subsequently correlated with the succession identified in the OCM. TD reveals an 80 cm-thick unit deposited within a narrow conduit, featuring three scours on bedrock correlated with distinct sedimentary episodes (Fig. 7). The confined morphology suggests that deposition was strongly influenced by channelled flows.

The TD stratigraphic succession comprises 5 vertically stacked units (SUs 36-37-38-39-40) that show massive and laminated fine-grained sediments. The passage among these units can be locally gradually or sharp.

SU 36 consists of dark brown silty clay with a weak sub-angular blocky structure and scattered centimetric limestone clasts at the top, becoming laminated and sandier toward the base (Fig. 7). SU 37 fills a concave erosional depression and is composed of pale brownish-grey silty clay with yellowish mottles and moderate blocky structure; a large limestone block ais embedded. SU 38 forms the main clay-rich cave fill and is subdivided into three sub-units, with massive structure. In SU 38b, discontinuous charcoal laminae occur. SU 39 occupies a shallow erosional depression within SU 38b and is made up of yellowish-brown, weakly laminated clayey silt with dispersed charcoal and a fine sand lens at the bottom. At the base, SU 40 fills a narrow erosional trough incised into SU 38c and consists of black to dark brown silty clay with a massive structure and abundant charcoal (Fig. 7).

### 6.2. Sedimentological, geochemical, and micropaleontological analyses

The sedimentological and geochemical characterisation of TB was carried out on the eight sedimentary units (SUs 12 to 60).

The general trend in GS analyses along the TB section (Fig. 8A) indicates that the upper part of the profile, corresponding to SU 12 and SU 25, is dominated by sandy-sized particles. In these units, sand is the main fraction, with silt and clay occurring in minor proportions. However, a marked increase in fine particles is recorded at the top and base of SU 12. From the base of SU 26 downward, there is a gradual increase in clay and

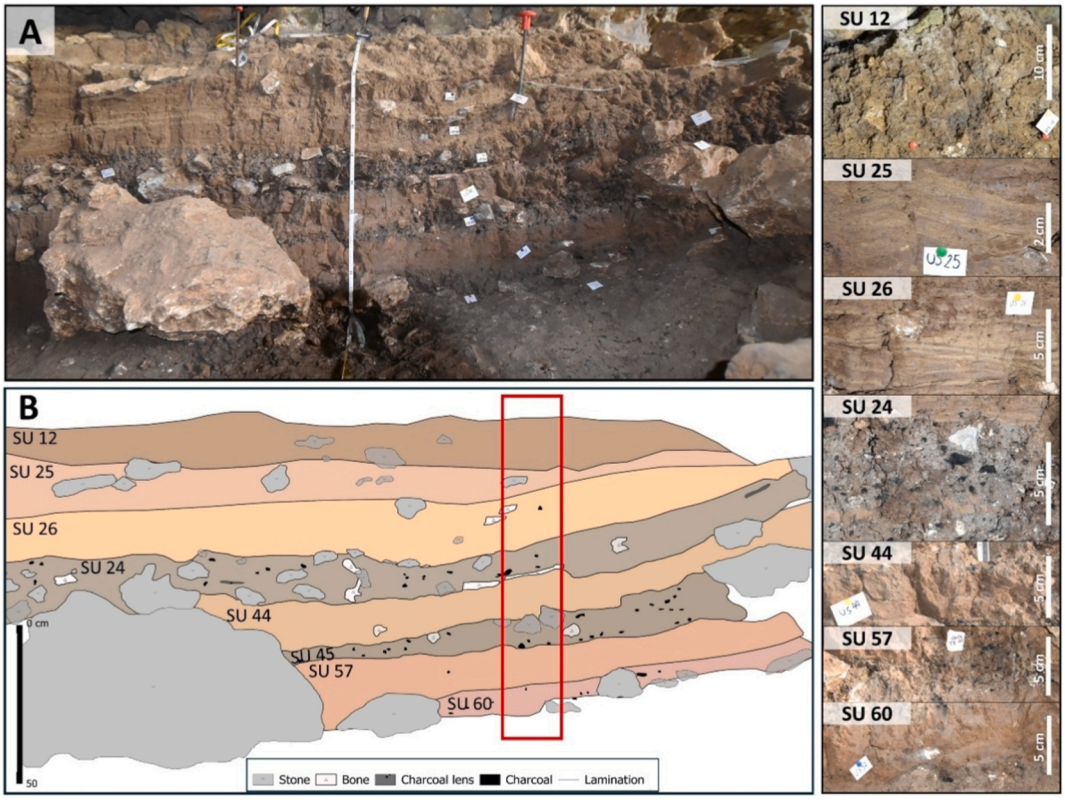


**Fig. 6.** A) Photograph of the TB section. B) Line drawing of the TB section showing the internal stratigraphic units; the red box indicates the position of the stratigraphic log in Fig. 8. The adjacent panels show close-up photographs of the individual stratigraphic units (SUs), as described in Section 6.1.

silt, which become the dominant components of the sediment throughout the rest of the succession. A fine-grained GS characterizes all underlying units. A localised increase in sand is observed at the base of SU 44, where the sandy fraction temporarily rises before the return to a predominantly silty-clayey matrix.

Within SU 24, a distinct and localised increase in gravel content is recorded, clearly standing out against the overall fine-grained background.

From the top of the succession down to 70 cm, including SU 12, SU 25, and SU 26, TOC and TIC remain relatively stable, with moderate values and no marked fluctuations. At SU 24, both TOC and TIC begin to increase, with TOC reaching its main peak and TIC at the SU 24–SU 44 boundary. Within SU 44, both TOC and TIC decrease markedly. In SU 45, TIC increases moderately, while TOC rises sharply between 90 and 100 cm, reaching a second high peak. In SU 57, both TOC and TIC decrease again, reaching their lowest values in the lower part of the profile (Fig. 8A).

Compositional analysis indicates that the samples from the TB section (TB40 and TB50) display a sedimentaclastic, feldspatho–quartzo–lithic composition with a clear dominance of monomineralic grains (>50%), mainly quartz and feldspar. Lithic grains form a subordinate component composed mainly of micritic to sparitic carbonate fragments, partly silicified, together with minor siltstone and argillite, and rare felsic volcanic lithics. Accessory minerals include micas (muscovite and biotite <0.8%) and opaque heavy minerals (<1.6%), whereas bioclasts and organic debris (gastropod fragments, coprolites, bone, and charcoal) are rare (<1%). Intrabasinal components are abundant (IL = 30–39%), mainly calcareous tufa intraclasts, clay–silt aggregates, and mud clasts (Fig. 10). The recalculated framework composition (QFL) indicates quartz contents between 54 and 64%, feldspar 24–31%, and lithic fragments 11–15%. Monocrystalline quartz (Qm = 60–70%) dominates, and feldspars are largely plagioclase-rich (KF/(KF + P) ≈ 0.33–0.35). Lithic fragments (L) account for less than 15% of framework grains and are overwhelmingly sedimentary (Ls = 85–100%), with rare volcanic fragments (Lm < 7.4%, Lv < 8.7%).

X-ray diffraction analysis of samples from trench TB reveals the presence of quartz, K-feldspars, plagioclase, and hydrous micas (muscovite and/or illite; see also Thompson and Ukrainczyk, 2002). Calcite is detected in all samples except TB 40, where the absence of the characteristic peak at ~29.4° 2θ indicates it lacks. The relative intensity of this peak varies across the TB section, suggesting differences in calcite abundance. A weak, broad peak around 12° 2θ in sample TB 100 may also indicate the presence of kaolinite (Fig. SI2).

The micropaleontological analysis on 24 samples from TB section indicates that the basal portion of the succession, from samples from 55 cm to 115 cm and 45 cm to 0 cm was barren. Sample from depth 50 cm revealed an abundant ostracod assemblage, dominated by *Ilyocypris bradyi*, with *Candona* sp., *Bithynia* fragments, and opercula also present (Fig. SI3).

The general trend in GS results along the TD section (Fig. 9B) shows that SU 36 is characterised by fine-grained sediments, with silt and clay as the dominant fractions at the top and a moderate presence of sand at the bottom. In SU 37, the GS becomes more heterogeneous, with higher sand proportions and a decrease in clay, while silt remains consistently present. A return to fine GSs is observed in SU 38a, where the sediments are predominantly composed of silt and clay with a degree of sand content. In SU 39, a slight coarsening trend is evident, with an increase in the sandy fraction and a concurrent decrease in silt, while clay remains stable. At the base of the profile, SU 40 is almost entirely composed of fine sediments, with a strong dominance of silt and clay and very low sand content.

From the top of the section to the base of SU 36, TOC values are moderate and stable, while TIC remains consistently low. In SU 37, TIC shows a marked increase, reaching its highest values in the profile, whereas TOC remains low throughout the unit. In SU 38a, TOC values are stable and slightly higher than in the overlying unit, while TIC

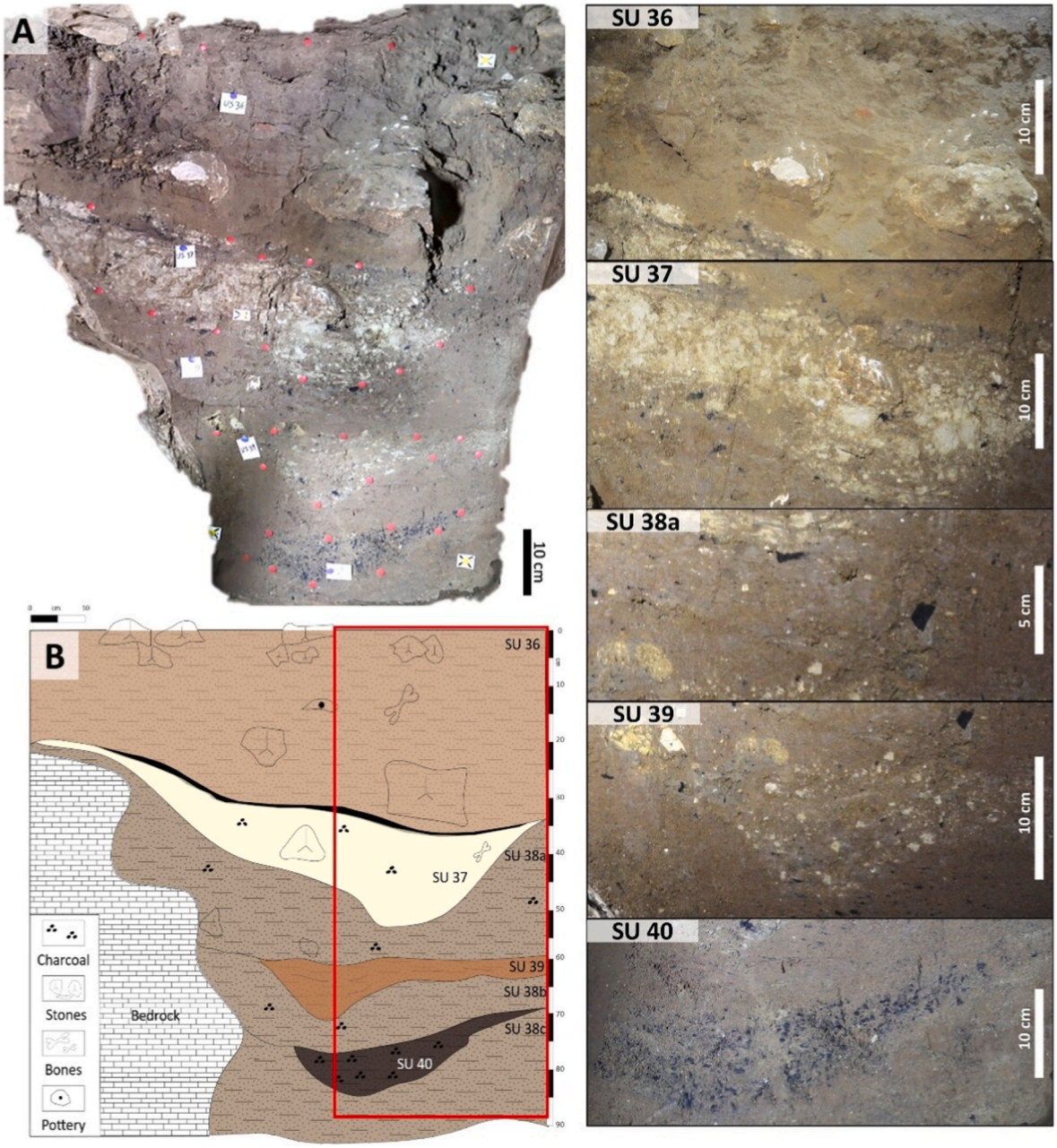


**Fig. 7.** Exposed stratigraphic succession of the TD section. Photo (A) and interpretative drawing (B) of the section TD; the red box indicates the position of the stratigraphic log in Fig. 8. The adjacent panels show close-up photographs of the individual stratigraphic units (SUs), which are described in detail in Section 6.1.

decreases but still shows moderate variability. In SU 39, TOC reaches its peak in the profile, while TIC remains moderate and stable. At the base of the sequence, in SU 40, TIC values decrease to their lowest levels, while TOC remains relatively low but exceeds TIC (Fig. 8B).

From a compositional point of view the TD70 sample exhibits a feldspathic–quartzose–lithic framework dominated by sedimentary lithics. Monocrystalline quartz (Qm = 62.2%) remains the main framework grain, while feldspar shows KF/P (K-feldspar/plagioclase) ratio of 0.48. Lithic fragments are exclusively sedimentary (Ls = 100%), comprising micritic and sparitic carbonates, minor clayey siltstone, and reworked pedogenic aggregates. Intrabasinal grains are particularly abundant (IL ≈ 57%), dominated by tufa and mud intraclasts, clay aggregates, and nodules, which locally obscure the primary depositional fabric. Accessory phases include rare micas (<1%) and sporadic opaque minerals, while bioclasts and organic remains are virtually absent. The recalculated QFL and QmKP proportions are Q = 61%, F = 33%, L = 6% and Qm = 62%, KF = 18%, P = 20%, respectively. The TD deposits differ markedly, being intrabasinally dominated and characterized by abundant carbonate intraclasts and tufa fragments (Fig. 9).

X-ray diffraction analysis reveals a slightly more complex mineralogical assemblage compared to TB (Fig. 8). Quartz and hydrous micas (muscovite/illite) are consistently present, with K-feldspars also detected except in TD 40. Unlike TB, plagioclase is absent in TD 10, TD 20, and TD 40. Weak, broad peaks at ~12° 2θ in TD_50 to TD_80 suggest possible kaolinite presence (Fig. 9). Calcite, identified mainly via the (104) reflection (~29.4° 2θ), is absent in TD 10 and TD 70, and only weakly present in TD 30. Conversely, it dominates in TD 40, where additional reflections [(012), (006), (202)] confirm its abundance. In this sample, only quartz, hydrous micas, and calcite were identified, indicating a distinct mineralogical composition (Fig. SI2).

In Trench TD, 13 samples were analysed for their micropalaeontological content. The lowermost part of the sequence was

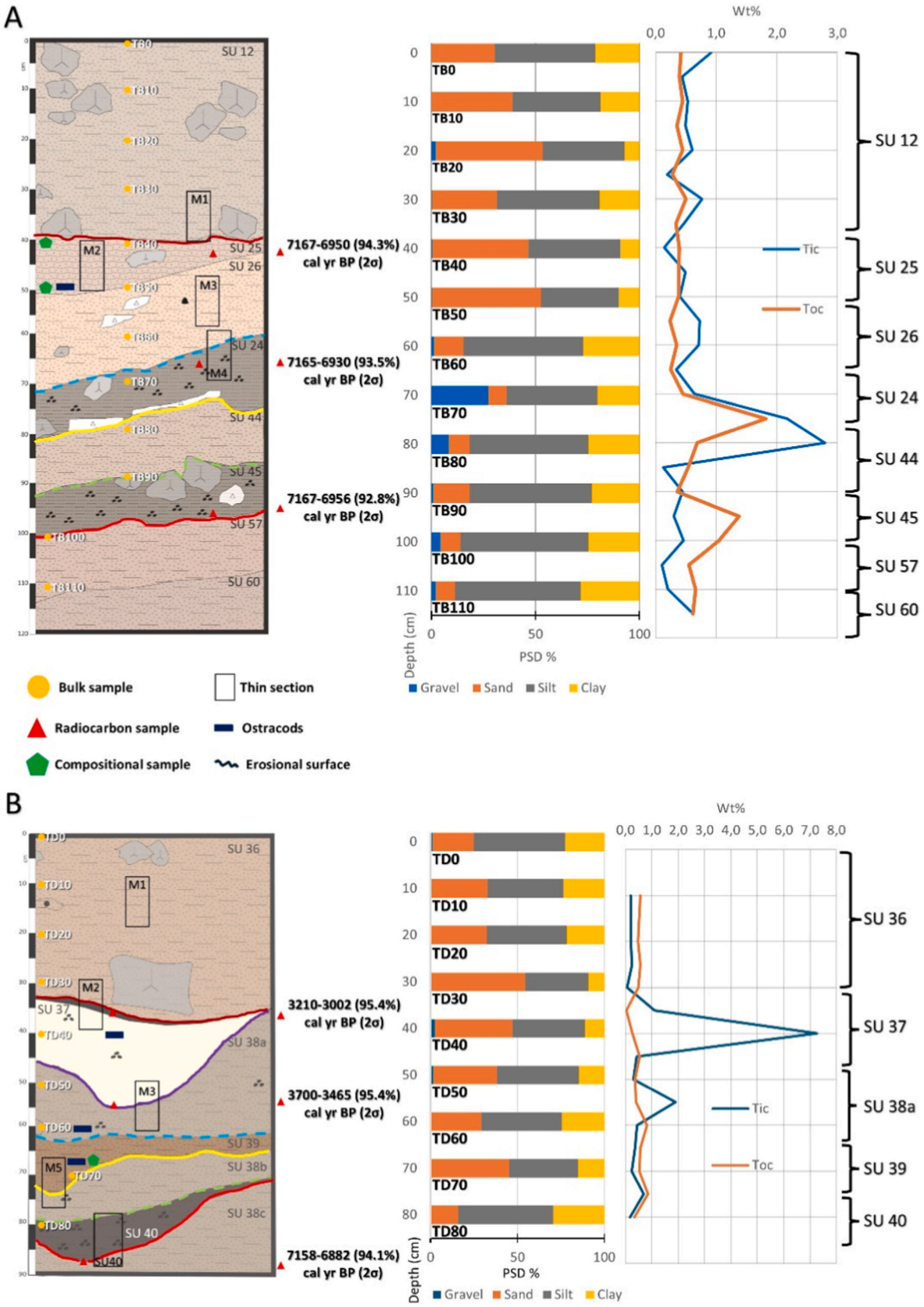


**Fig. 8.** Stratigraphic succession of TB (A) and TD (B) sections with associated micromorphological and compositional samples, radiocarbon dates, particle size distribution (PSD), samples with ostracods and carbon content (TIC and TOC). The coloured lines on sections TA and TB indicate the correlating surfaces common to both. Coloured lines highlight the main stratigraphic surfaces identified in the TB and TD sections and are used to facilitate correlation between the two trenches. Solid lines represent erosional surfaces, whereas dashed lines indicate depositional contacts between stratigraphic units.

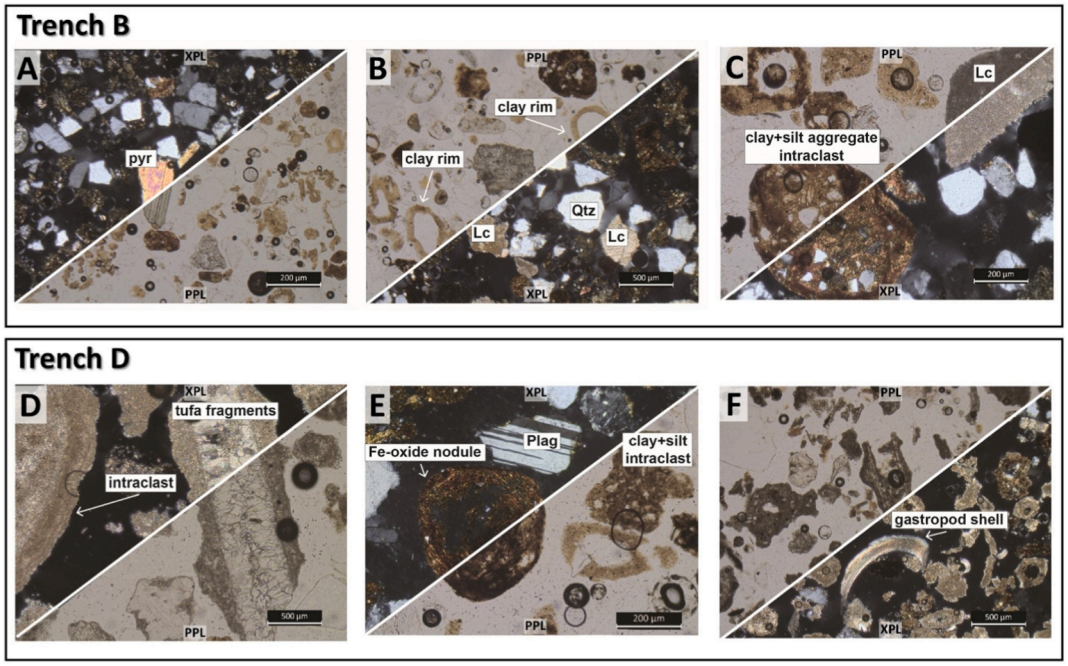


**Fig. 9.** Photomicrographs of sand-sized deposits from Battifratta Cave. (A–C) Samples from Trench B (TB40–TB50) showing the predominance of extrabasinal siliciclastic grains and clay-related pedogenic features. Monomineralic grains include quartz (Qtz), feldspar (KF), and minor volcanic lithics (Lv). Lithic fragments (Lc, Lsa) are mainly micritic to sparitic carbonate grains, partly silicified. Common features include clay rims surrounding detrital particles, clay–silt aggregates, and pyr (pyroxene) grains, indicating limited transport and post-depositional alteration. Clay coatings and sericite rims document *in situ* weathering and redistribution within the upper cave–soil interface. Scale bars: 1 mm and 200 μm. (D-F) Samples from Trench D (TD 70) characterized by abundant intrabasinal carbonate grains, including tufa and travertine fragments, calcitic intraclasts, and clay–silt aggregate intraclasts. Detrital quartz, feldspar (Plag) and carbonate lithic fragments (Lc) are sparse and typically coated by clay films. Locally, Fe-oxide nodules and gastropod shell fragments occur within the micritic matrix. The predominance of reworked tufa fragments, peloids, and intraclasts reflects low-energy sedimentation in cave pools and episodic roofspall reworking. Scale bars: 500 μm and 200 μm.

barren, but beginning at approximately 70 cm depth the deposits yielded layers rich in plant remains and *Bithynia opercula*. The sample taken at 65 cm contained a well-developed ostracod assemblage dominated by *Cyprideis torosa*, representing a distinctly oligotypic community. Samples between 60 cm and 50 cm similarly produced plant debris together with abundant *Bithynia opercula* (Fig. SI3). A marked environmental shift is evident in the sample at 40 cm, which contains abundant carbonate concretions and a microfossil assemblage dominated by *Candona angulata* along with numerous charophyte gyrogonites.

### 6.3. Micromorphological investigation

#### 6.3.1. Thin sections from TB

Micromorphological analyses of the selected SUs of section TB are summarized in Table 1, whereas main aspects are reported in the following part. The coarse mineral fraction is consistent throughout the succession, with a prevalence of subangular and subrounded sand-sized quartz grains followed by other fine-grained siliceous and volcanic mineral grains inherited by the local lithologies and soil cover, namely chert, orthopyroxenes, feldspars, and micas. Their input within the cave is compatible with interstitial colluvium washing the particles downwards through the fissures in the travertine bedrock, with relative abundances varying slightly, likely because of ultra-local variations in their availability. Heterometric travertine fragments showing varying degrees of roundedness and solutional alteration are common throughout the deposit.

Organic inclusions are dominated by heterometric charcoal fragments ranging from silt size to sub-centimetric, generally subangular to subrounded due to water traction and mostly situated within SU 24 (partially eroded and redeposited at the bottom of SU 26). Bone fragments exist in varying concentrations and are generally sand- and gravel-sized and sometimes burned and phosphatised. However, the larger diagnostic osteological remains were mostly recovered during archaeological excavation for dedicated processing. Small ceramic fragments and lumps of grog and partially fired clay are sometimes observed in association with bone-bearing layers, but likewise, the larger fragments were collected during excavation. Lesser amounts of shell fragments (terrestrial gastropods) and phosphatised coprolite fragments (unidentified) are found in association with the former elements.

The analysis of the groundmass revealed a hidden feature related to the overall accretion of the deposit: the fine-grained fraction identified with the GS analysis (clay silt) is composed of rounded aggregates highly varying in size (medium sand up to centimetric) divided into a light yellow (Type 1) and a dark brown (Type 2) variants, interpreted as two separate kinds of pedorelicts. These two intermix, producing an overall yellowish brown groundmass colour throughout the succession. Their provenance, as for the coarse mineral grains, is to be reconducted to karst dynamics and sediment source. Type 1 pedorelicts are interpreted as rip-up clasts eroded by flowing water from the sediment deposits found in cave interior conduits (Fig. 3). Type 2 pedorelicts reflect colour and textural characteristics typical of humic soils and likely inherited from the overlying soil cover injected from the epikarst. Type 1 and 2 pedorelicts display a certain degree of mechanical durability, as they can be observed as discrete textural entities that became part of the very depositional structures of the layers. This is extremely evident, for example, in the upper half of thin section TB M2 (Fig. 10A–C), where they associate with mineral grains to form well-preserved fining-upwards trends created by low-energy water discharge at the outlet of the cave (Fig. 10B).

Primary depositional structures, however, have been locally disturbed by compaction and anthropic presence that resulted in partial welding of pedorelicts (Fig. 10D and E), heavy deformation of the deposits, and enrichment in charcoal, bone fragments, and the other

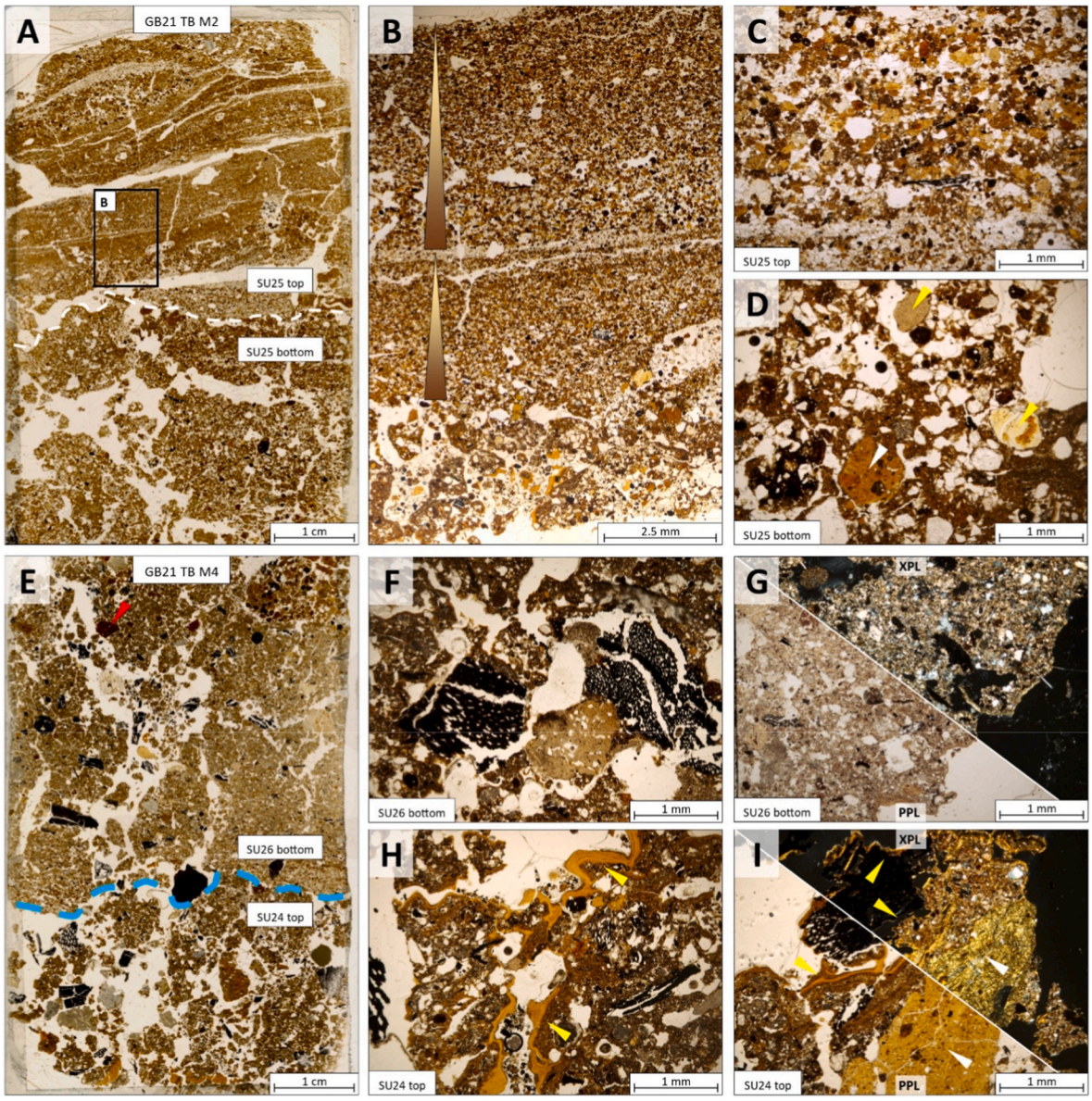


**Fig. 10.** Selected thin section scans and microphotographs from section TB. A) Scan of sample GB21 TB M2 comprising the upper and lower portions of SU 25. The white dashed line indicates a stratigraphic transition identified in thin section but not during excavation and sampling. Slack water laminae and fining-upward trends are recognizable in the upper half, while the lower half is characterised by fragmented and loosely packed aggregates of welded and vughy silty clay. Note the desiccation fissures in the laminated deposit, accompanied by degassing vesicles, and the loose chaotic packing void in the lower-level B) Magnified detail of fining-upward structures in SU 25 top, indicated by the upright arrows. C) Plane polarized light (PPL) detail of the Type 1 and 2 rounded pedorelicts (yellow and brown, respectively) constituting the fining-upwards structures of SU 25, in association with same-sized mineral grains dominated by quartz. D PPL detail of SU 25 bottom. The deposit is composed of welded brown clay speckled with brighter-coloured Type 1 pedorelicts (white arrow) and enriched with transport-rounded biogenic components such as the bone fragment and presumed phosphatised coprolite (yellow arrows). E) Scan of sample GB21 TB M4 comprising the bottom of SU 26 and the top of SU 24, separated along a probable erosion/frequentation surface. The blue dashed line refers to the same discontinuity reported in Fig. 8. Both SUs are characterized by loosely packed subrounded silty clay aggregates and abundant charcoal, bone fragments, and anthropogenic material, such as the red ceramic fragments at the top of the section (red arrow). F) PPL detail of SU 26, showing charcoal with a rounded and altered bone fragment (centre of the picture). G-I) PPL/XPL details of SUs 26 24, showing a localized and partially mineralized ash deposit (G), convoluted laminated clay coatings within channels and chambers (yellow arrows) (H), and a large Type 2 pedorelict (white arrow), welded with brown clay aggregates and charcoal, and collectively wrapped in laminated clay coatings (yellow arrows) (I).

biogenic and anthropogenic elements previously described (thin section TB M4, Fig. 10F–J). Clay dissolution caused by ambient water (likely dripwater) contributed to the partial textural, structural, and chromatic homogenization of the same layers (Fig. 10G–I).

Porosity is high throughout the deposit, expressed as planes and fissures with rare vughs and vesicles in the laminated strata reflecting desiccation, textural discontinuities, and syn-depositional incomplete degassing (Fig. 10A), and packing voids and bioturbative channels and chambers in the anthropized layers (Fig. 10E).

### 6.3.2. *Thin sections from TD*

Micromorphological analyses of the selected SUs of section TD (Table 2), as for those of section TB, corroborate field observations and find remarkable correlation with the former, albeit with slight structural differences imparted by local channelization (Fig. 7).

The coarse mineral fraction is again consistent throughout the

**Table 1**
*Micromorphological descriptions of the TB section. Particle size and frequency of components are reported after* Stoops (2021) *as follows.* SIZE: G (gravel); VC (very coarse sand); C (coarse sand); M (medium sand); F (fine sand). FREQUENCY: + (very few); ++ (few); +++ (common); ++++ (frequent).

| Sample | SU | Mineral coarse components | Biogenic and anthropogenic coarse components | Groundmass | Voids | C/F related distribution, B-fabric | Aggregation, microstructure | Pedofeatures and sedimentary features |
|---|---|---|---|---|---|---|---|---|
| **GB21 TB M1** | 12 | Quartz (M) ++++<br>Limestone fragments (G to F) +++<br>Chert fragments (M to F) +<br>Volcanic minerals (ortopx, K-felsp, micae)(M to F) ++ | Bone fragments (M to VF) +<br>Charcoal (M to F) + | Yellowish brown silty loam | Channels +<br>Structural +++<br>Vughs +++ | Close to double spaced porphyric Crystallitic | Moderate Vughy | Illuviation clay coatings with internal convolute laminations ++<br>Pedorelicts:<br>1) Brown subrounded clay aggregates (infiltrated organic soil fragments) (M to F) +<br>2) Yellow rounded clay aggregates (endogenic rip-up clasts) ++<br>Rolled Fe-Mn nodules (cs -fs) +++ |
| **GB21 TB M2a** | Top 25 | Quartz (VC to F) ++++<br>Limestone fragments (G to F) +++<br>Chert fragments (M to F) +++<br>Volcanic minerals (ortopx, K-felsp, micae)(F) ++ | Bone fragments (M to VF) +<br>Microcharcoal (F to VF) ++++<br>Charcoal (M to F) +++<br>Plant remains + | Yellowish brown sandy loam | Channels ++<br>Structural +++<br>Vesicles +++<br>Planes +++ | Double space porphyric, locally monic Crystallitic, locally speckled | Well developed Angular blocky to platy | Fining upward sequences composed of medium to fine mineral sand and silt, and sorted rounded pedorelicts<br>Pedorelicts:<br>1) Brown subrounded clay aggregates (infiltrated organic soil fragments) (M to F) +++<br>2) Yellow rounded clay aggregates (endogenic rip-up clasts) ++++<br>Illuviation clay coatings +<br>Rolled Fe-Mn nodules (cs -fs) +++ |
| **GB21 TB M2b** | Bottom 25 | Quartz (VC to F) ++++<br>Limestone fragments (G to F) +++<br>Chert fragments (M to F) +++<br>Volcanic minerals (ortopx, K-felsp, micae)(F) ++ | Bone fragments (M to VF) +<br>Microcharcoal (F to VF) ++++<br>Charcoal (M to F) +++<br>Non combusted plant remains +<br>Ceramic fragments + | Yellowish brown sandy loam | Channels ++<br>Structural +++<br>Vesicles +++<br>Planes +++ | Double space porphyric, locally monic Crystallitic, locally speckled | Well developed Angular blocky | Illuviation clay coatings: ++<br>Pedorelicts:<br>1) Brown subrounded clay aggregates (infiltrated organic soil fragments) (M to F) ++<br>2) Yellow rounded clay aggregates (endogenic rip-up clasts) +++<br>Rolled Fe-Mn nodules (cs -fs) +++ |
| **GB21 TB M3** | Top 26 | Quartz (VC to F) ++++<br>Limestone fragments (G to F) +++<br>Chert fragments (M to F) +++<br>Vulcanic minerals (ortopx, K-felsp, micae)(F) ++ | Bone fragments (G to M) ++<br>Charcoal (M to F) +++<br>Shell fragments ++<br>Ceramic fragments locally burned (G to VC) + | Dark yellowish brown sandy loam | Channels ++<br>Chambers +++<br>Structural +++ | Close to open porphyric Speckled, locally crystallitic | Well developed, Subangular blocky | Illuviation clay coatings ++<br>Pedorelicts:<br>1) Brown subrounded clay aggregates (infiltrated organic soil fragments) (M to F) ++<br>2) Yellow rounded clay aggregates (endogenic rip-up clasts) +++<br>Rolled Fe-Mn nodules (cs -fs) +++ |
| **GB21 TB M4a** | Bottom 26 | Quartz (C to F) +++<br>Limestone fragments (G, VC to F) +++<br>Chert fragments ++<br>Volcanic minerals (ortopx, K-felsp, micae)(M to F) ++ | Bone fragments (G to MS) ++<br>Charcoal (G to F) ++++<br>Coprolite fragments (G to MS) +<br>Shell fragments +<br>Ceramic fragments +<br>Plant remains ++<br>Grog paste + | Dark yellowish brown sandy loam | Chambers ++++<br>Vesicles ++++<br>Structural ++++<br>Planes +++ | Open to close porphyric Crystallitic | Weakly developed Subangular to crumby | Illuviation clay coatings with internal convolute laminations +++<br>Infilling of voids (bioturbation)<br>Pedorelicts:<br>1) Brown subrounded clay aggregates (infiltrated organic soil fragments) (M to F) +<br>2) Yellow rounded clay aggregates (endogenic rip-up clasts) +++<br>Rolled Fe-Mn nodules (cs -fs) + |
| **GB21 TB M4b** | 24 top | Quartz (C to F) +++<br>Limestone fragments (G, VC to F) +++<br>Chert fragments (G to M) +<br>Volcanic minerals (ortopx, K-felsp, micae)(F) + | Bone fragments locally burned (G to MS) +<br>Charcoal (CS to F) ++++<br>Microcharcoal (F to VF) +++<br>Local ash accumulations + | Brown sandy loam | Chambers +++<br>Vesicle +++<br>Structural +++<br>Moldic ++ | Open to close porphyric Crystallitic, locally speckled | Weakly developed Crumby to spongy | Illuviation clay coatings with internal convolute laminations ++<br>Pedorelicts:<br>1) Brown subrounded clay aggregates (infiltrated organic soil fragments) ++<br>2) Yellow clay aggregates (endogenic rip-up clasts), large and deformed by |

(*continued on next page*)

**Table 1** (*continued*)

| Sample | SU | Mineral coarse components | Biogenic and anthropogenic coarse components | Groundmass | Voids | C/F related distribution, B-fabric | Aggregation, microstructure | Pedofeatures and sedimentary features |
|---|---|---|---|---|---|---|---|---|
| | | | Ceramic fragments (G to VC) ++ | | | | | diagenesis and mechanical pressure<br>Rolled Fe-Mn nodules (cs -fs) + |

succession with the same characteristics as section TB, dominated by sand-sized subangular to subrounded quartz grains in varying proportions with lesser fine-grained siliceous and volcanic mineral grains inherited from the epikarst.

Type 1 and 2 pedorelicts are dominant in the making of the groundmass. In the upper strata, these form highly porous deposits with a fining-upward trend and with occurrence of chitonic clay pellicles produced by slight clay illuviation coating mineral grains and pedorelicts (Fig. 11A and B). Conversely, in the lower strata they appear constipated, deformed, and welded together, with convoluted and laminated clay illuviations partially filling bioturbative voids and still producing chitonic pellicles coating surviving individual grains and aggregates (Fig. 11E–L). Contact surfaces between SUs are slanted as a result of channelization and confinement, sometimes presenting localised slickensides resulting from compaction along tilted planes. Charcoal fragments occur in tight correlation with section TB, with the highest concentration found in SU 40 (corresponding to section TB's SU 45). As will be further explored in the Discussions, charcoal is likely entering the cave together with interstitial soil colluvium from the epikarst, deriving from episodes of forest fires that promoted slope erodibility and enhanced downward charcoal-enriched sediment flux. Other biogenic and anthropogenic components remain present, yet in overall lesser amounts compared to section TB because of the greater distance from the main occupation area of the cave. SU 37 (Fig. 11 A–C-D) has a different composition, being a deposit of dissolved and re-cemented travertine that produced a channel-confined crust of limestone micrite with a very limited content of coarse mineral grains. The crust has a massive structure and a high content of broken and dispersed gastropod shell fragments, especially in its upper stratigraphic interface, where the still soft micrite mingles with the incoming sediment, forming SU 36, producing interdigitated horizontal platy structures. This suggests the temporary permanence of a confined small pond of lime-saturated water, followed by precipitation of micrite, later buried by an endokarst discharge event before complete solidification.

#### 6.3.3. *Thin section analyses of the combustion feature*

In addition to the Neolithic sequence, the archaeological levels attributed to the Bronze Age were also investigated. Evidence related to this phase is spatially restricted and concentrated in a limited area of the cave entrance. This area corresponds to the channel associated with the water outspring, developed during a phase of karstic reactivation affecting the cave mouth (Figs. 2 and 4).

Within this sector, an anthropogenic structure was identified and documented. The feature, stratigraphically defined as SU 43, cuts into the uppermost portion of SU 24. It consists of a shallow sub-circular negative structure containing abundant burnt material and has been reported during excavation as a combustion feature (Fig. 12). Micromorphological analyses of SU 43 identified abundant burnt macrobotanical remains, taxonomically attributed to Acer sp., Fraxinus sp., Ostrya carpinifolia, and Quercus ilex (Conati Barbaro et al., 2024a). Observation under the microscope revealed also burnt bone fragments, rubified rock clasts, ash-rich lenses, and compacted burnt dung remains (Fig. 12F and G). The latter were identified through the presence of siliceous plant fibres associated with faecal spherulites (Fig. 12G), which are diagnostic of bovids and ovicaprines (Canti, 1997).

### 6.4. *Radiocarbon dating*

In Trench B, 4 radiocarbon dates from charcoal and one from bone were analysed.

A charcoal sample from SU 26 (LTL22173) gave a calibrated age of 7167–6950 cal yr BP (2σ), while a second charcoal sample from SU 24 (LTL22174) returned 7165–6930 cal yr BP (2σ). Charcoal from SU 45 (LTL31725) was dated to 7167–6956 cal yr BP (2σ). A bone fragment from the bottom of SU 60 (LTL33852) provided a consistent result of 7165–6940 cal yr BP (2σ). Also sample from the top of SU 24 (LTL22170), dated to 3454–3332 cal yr BP (2σ) (Table 3).

In Trench D, charcoal from the top of SU 37 (LTL22169) yielded an age of 3210–3002 cal yr BP (2σ), while a sample from the bottom of the same unit (LTL22175) gave 3700–3465 cal yr BP (2σ). Charcoal from the bottom of SU 40 (LTL22171) was dated to 7158–6882 cal yr BP (2σ) (Table 3).

The most recent archaeological chronology is based on the analysis of pottery, namely a 16th century CE maiolica jug recovered from the upper units, which provide a terminus post quem for this phase (Fig. 4).

## 7. Discussion

### 7.1. *Evolution and formation of the Middle Holocene deposit*

The Middle Holocene sedimentary infill of Grotta Battifratta reflects the interplay between karstic processes, hydroclimatic fluctuations, and anthropogenic activity. Stratigraphic records from the inner and outer cave mouth sectors document short-lived depositional and erosional phases during the Middle Neolithic (7165–6882 cal yr BP) with episodic human occupation, abandonment, external disturbance, and sediment remobilization. Radiocarbon dates indicate a brief and intense sedimentary phase, reflecting a local example to regional climatic variability and land use from the Neolithic onward (Kelly and Huntley, 1991; Mercuri et al., 2002; Colombaroli et al., 2007; Drescher-Schneider et al., 2007; Vigliotti et al., 2010; Vannière et al., 2008; Brown, 2013; Stoddart et al., 2019).

At the base of the successions, SU 38c (TD) and SUs 57 and 60 (TB), analyses highlighted slope wash events that transported mature, pedogenised soils aggregates into the cave through a combination of gravitational fast to slow soil injection, surface runoff, and epikarstic percolation that winnowed the fine particles (see e.g., Ford and Williams, 2007; Sasowsky and Mylroie, 2007). The deposition occurred in a ponding setting fed by dripwater, and seasonal discharge favoured the development of slack-water sedimentary facies (Fig. 13A). As external sedimentary flow or soil injection entered the cave, it moved from narrow internal joints, fractures and conduits (inner cave mouth) to the broader outer cave mouth sector, where collapse roofspall blocks and ramp-like morphologies acted as sediment traps, leading to the deposition of laminated sediments promoted by gradual energy dissipation.

A subsequent erosional phase is evident as a shallow scour at the base of SU 40 (TD) and as an erosional surface in SU 45 (TB) (Fig. 13B). Brown soil round aggregates dominates the groundmass composition of SU 40, and the absence of fine-grained slack water laminations testifies high-energy chaotic releases (Fig. 11J–L). The great amount of large and rounded charcoal fragments embedded within this deposit may attest the occurrence of forest fires in the catchment area of the cave,

**Table 2**
*Micromorphological descriptions of the TB section. Particle size and frequency of components are reported after* Stoops (2021) *as follows.* SIZE: G (gravel); VC (very coarse sand); C (coarse sand); M (medium sand); F (fine sand). FREQUENCY: + (very few); ++ (few); +++ (common); ++++ (frequent).

| Sample | SU | Mineral coarse components | Biogenic and anthropogenic coarse components | Groundmass | Voids | C/F related distribution, B-fabric | Aggregation, microstructure | Pedofeatures and sedimentaryfeatures |
|---|---|---|---|---|---|---|---|---|
| **GB21 TD M1** | 36 | Quartz (M to F) +++<br>Limestone fragments (C to F), ++<br>Chert, locally burned (M to F) +++<br>Volcanic minerals (ortopx, K-felsp, Micae) (M to F) ++ | Bone fragments (M) +<br>Charcoal (C to F) +++<br>Shell fragments ++<br>Ceramic fragments + | Yellowish brown silty loam | Compound packing voids +++ | Monic to close porphyric Crystallitic | Moderate Crumby to sub-angular blocky | Illuviation clay coatings with internal convolute laminations ++++<br>Pedorelicts:<br>1) Brown subrounded clay aggregates (infiltrated organic soil fragments) (M to F) + +<br>2) Yellow rounded clay aggregates (endogenic rip-up clasts) +++<br>Rolled Fe-Mn nodules (cs -fs) +++ |
| **GB21 TD M2a** | 36 bottom | Quartz (M to F) +++<br>Limestone fragments (C to F), ++<br>Chert, locally burned (M to F) +++<br>Volcanic minerals (ortopx, K-felsp, Micae) (M to F) ++ | Bone fragments (M) +<br>Charcoal (C to F) +++<br>Shell fragments ++<br>Ceramic fragments + | Yellowish brown silty loam | Compound packing voids +++ | Monic to close porphyric, locally chitonic Crystallitic | Moderate Crumby to sub-angular blocky | Illuviation clay coatings with internal convolute laminations +++<br>Pedorelicts:<br>1) Brown subrounded clay aggregates (infiltrated organic soil fragments) (M to F) +++<br>2) Yellow rounded clay aggregates (endogenic rip-up clasts) ++++<br>Rolled Fe-Mn nodules (cs -fs) ++ |
| **GB21 TD M2b** | 37 top | Quartz (M to F) ++++<br>Limestone fragments, locally weathered (C to F), ++++<br>Chert (M to F) ++<br>Volcanic minerals (ortopx, K-felsp, Micae) (M to F) + | Bone fragments (G) +<br>Charcoal (G to M), angular and locally fragments +++<br>Coprolite fragments +<br>Shell fragments + | Light greyish brown silty loam and micrite | Chambers ++<br>Structural +++<br>Planes ++<br>Channels + | Close porphyric, locally chitonic Speckled to crystallitic | Moderate Complex, crumby to sub-angular blocky and platy | Illuviation clay coatings with internal convolute laminations ++++<br>Pedorelicts:<br>1) Brown subrounded clay aggregates (infiltrated organic soil fragments) (M to F) ++<br>2) Yellow rounded clay aggregates (endogenic rip-up clasts) +++<br>Local fining-upward sequence of fine sand to silty clay +<br>Rolled Fe-Mn nodules ++ |
| **GB21 TD M2c** | 37 | Quartz (M to F) ++<br>Chert (M to F) ++ | Bone fragments (M to F) +<br>Charcoal (G to M) ++<br>Shell fragments +++ | Light yellowish grey micrite | Vughs +<br>Channels + | Open porphyric Crystallitic | Well developed Massive | Occasional clay papulae +<br>Rounded Fe-Mn nodules and zonal impregnation ++ |
| **GB21 TD M3a** | 37 bottom | Quartz (M to F) ++<br>Chert (M to F) ++ | Bone fragments (M to F) +<br>Charcoal (G to M) +++<br>Shell fragments ++ | Light yellowish grey micrite | Vughs +<br>Channels + | Open porphyric Crystallitic | Well developed Massive | Occasional clay papulae +<br>Rounded Fe-Mn nodules and zonal impregnation ++ |
| **GB21 TD M3a** | 38a top | Quartz (C to F) +++<br>Limestone fragments (G, VC to F) +++<br>Volcanic minerals (ortopx, K-felsp, Micae) (M to F) ++ | Bone fragments (G) ++<br>Charcoal (G to M) +++<br>Shell fragments ++ | Brown sandy loam | Chambers +++<br>Vesicles +<br>Structural +++<br>Planes +++ | Close to open porphyric Crystallitic, locally porostriated and granostriated | Well developed Subangular blocky | Illuviation clay-silt coatings ++<br>Pedorelicts:<br>1) Brown subrounded clay aggregates (infiltrated organic soil fragments) (M to F) +++<br>2) Yellow rounded clay aggregates (endogenic rip-up clasts) ++<br>Local fining-upward sequence of fine sand to silty clay +<br>Rolled Fe-Mn nodules ++++ |

(*continued on next page*)

**Table 2** (*continued*)

| Sample | SU | Mineral coarse components | Biogenic and anthropogenic coarse components | Groundmass | Voids | C/F related distribution, B-fabric | Aggregation, microstructure | Pedofeatures and sedimentaryfeatures |
|---|---|---|---|---|---|---|---|---|
| **GB21 TD M5a** | 39 | Quartz (M to F) ++++ Limestone fragments (G to F), ++++ Chert (M to F) + Volcanic minerals (ortopx, K-felsp, Micae) (F) + | Bone fragments (G to M) + Charcoal (G) + | Light brown sandy loam | Chambers ++ Channels + Structural +++ | Close porphyric Crystallitic | Weakly developed Crumby | Illuviation clay-silt coatings with internal convolute laminations +++ Pedorelicts: 1) Brown subrounded clay aggregates (infiltrated organic soil fragments) (M to F) + 2) Yellow rounded clay aggregates (endogenic rip-up clasts) + Slickensides + Rolled Fe-Mn nodules + Dissolution and micro-pitting of limestone fragments ++ |
| **GB21 TD M5b** | 39 bottom | Quartz (M to F) ++++ Limestone fragments (mainly travertine) (G to F), ++++ Chert (M to F) ++ Volcanic minerals (ortopx, K-felsp, Micae) (M to F) + | Charcoal (M to F) ++ Terrestrial gastropod shell fragments + | Brown silty loam | Structural +++ Chambers ++ | Single space enaulic, locally chitonic Random striated | Weakly developed Complex, vughy to crumb and chamber | Illuviation clay-silt coatings with internal convolute laminations ++++ Pedorelicts: 1) Brown subrounded clay aggregates (infiltrated organic soil fragments) (M to F) ++++ Rolled Fe-Mn nodules ++ |
| **GB21 TD M5c** | 38b top | Quartz (M to F) ++++ Limestone fragments (mainly travertine) (G to VC), +++ Chert (M to F) ++ Volcanic minerals (ortopx, K-felsp, Micae) (M to F) + | Charcoal (G, VCS to F) ++ | Light brown sandy loam | Chambers +++ Structural ++++ | Single space enaulic, locally chitonic Crystallitic, locally speckled | Weakly developed Complex, vughy to crumb and chamber | Illuviation clay-silt coatings with internal convolute laminations ++++ Pedorelicts: 2) Yellow rounded clay aggregates (endogenic rip-up clasts) +++ Rolled Fe-Mn nodules + |
| **GB21 TD M5d** | 38b | Quartz (C to F) ++++ Limestone fragments (M to F), +++ Chert (C to F) +++ Volcanic minerals (ortopx, K-felsp, Micae) (M to F) ++ | Charcoal (G to F) ++ | Brown silty loam | Chambers ++ Channels + Structural ++++ | Chitonic to double spaced coarse enaulic Granostriated | Moderate Bridged grain | Pedorelicts: 1) Brown subrounded clay aggregates (infiltrated organic soil fragments) (M to F) ++++ Rolled Fe-Mn nodules (m-f) ++ |
| **GB21 TD SU40** | 40 | Quartz (C to F) ++++ Limestone fragments (M to F), +++ Chert (C to F) +++ Volcanic minerals (ortopx, K-felsp, Micae) (M to F) ++ | Bone fragments (M to F) ++ Charcoal (C to F) ++++ | Dark brown silty loam | Chambers +++ Vesicles +++ Structural +++ | Close porphyric, locally chitonic Crystallitic | Moderate Chamber | Illuviation clay-silt coatings with internal convolute laminations +++ Pedorelicts: 1) Brown subrounded clay aggregates (infiltrated organic soil fragments) (M to F) ++++ 2) Yellow rounded clay aggregates (endogenic rip-up clasts) ++ Rolled Fe-Mn nodules (cs -fs) +++ |

promoting slope instability and remobilization of soil fragments and burnt plant remains (see e.g., Drescher-Schneider et al., 2007; Vannière et al., 2008; Stoddart et al., 2019). At current knowledge, whether such fires were spontaneous or intentionally produced to manage local deforestation, it is impossible to say.

A period of reduced water flow is observed in SU 38b (TD) and SU 44 (TB). These units exhibit well-laminated silts with minor sand and clay, scattered charcoal, and micromorphological features that are indicative

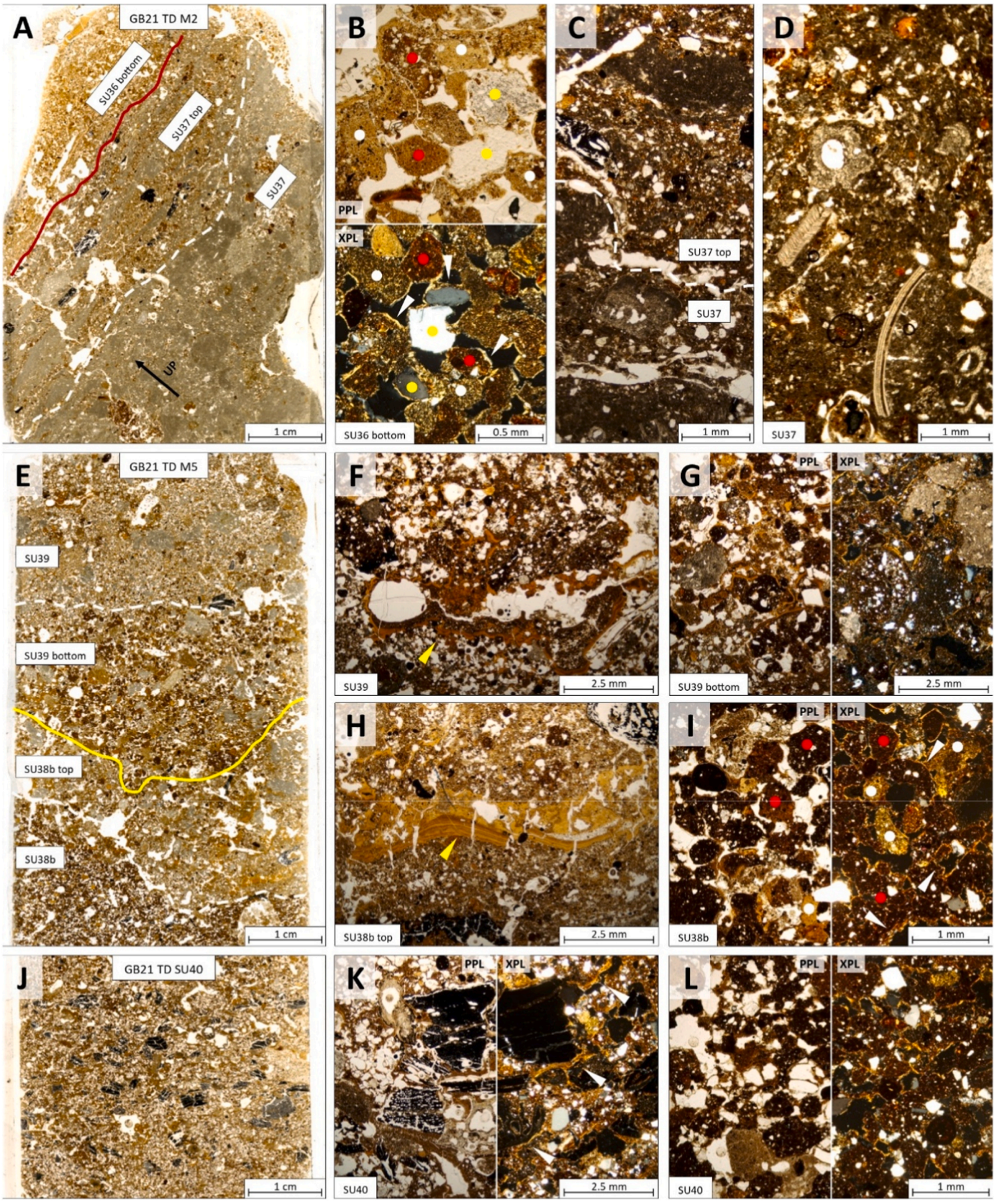


*(caption on next page)*

**Fig. 11.** Selected thin section scans and microphotographs from section TD. In the scans, the white dashed lines indicate a stratigraphic transition identified in thin section but not during excavation and sampling, and the coloured solid lines refer to the same discontinuities reported in Fig. 8. A) Scan of sample GB21 TD M2 comprising SU 37 and the lower portion of SU 36. "SU 37 top", as defined during excavation, is an interdigitation produced during the wet deposition and subsequent compaction of SU 36. B) Plane polarized and cross polarized light (PPL/XPL) detail of SU 36, composed of loosely packed Type 1 and 2 pedorelicts (respectively, white dots and red dots) and mineral grains (yellow dots) bound by a thin coating of highly birefringent chitonic illuvial clay (white arrows). C-D) PPL details of SU 37 and its contact zone with SU 36. Gastropod shells are very common in SU 37 (D), broken and dispersed within a low porosity micrite paste. E) Scan of sample GB21 TD M5 comprising the bottom of SU 39 and the top of SU 38b, each subdivided into 2 sub-layers recognized during micromorphological analysis. Throughout the layers, bone fragments and other biogenic components are rare, and charcoal/ashy spots occur occasionally. F-I) PPL/XPL details of section M5, showing common traits along the intercepted stratigraphy. (F) and (H) show a groundmass composed of homogenized Type 1 and 2 pedorelicts giving an overall light brown colour to the deposit, rich in mineral grains with dominant medium sand-sized quartz. Convoluted laminated clay coatings are common within large channels (yellow arrows). (G) and (I) show discrete Type 1 and 2 pedorelicts (respectively, white dots and red dots) with a dominance of the latter (brown clay aggregates), loosely packed and partially welded, bound by a thin coating of highly birefringent chitonic illuvial clay (white arrows). J) Scan of sample GB21 TD SU40 comprising SU 40 only. Large charcoal fragments are extremely common and represented the main marker for SU 40 during excavation. K) Detail of SU 40's charcoal fragments that appear well-integrated within the welded silty clay groundmass and coated by illuvial clay along structural voids (white arrows) shared with the welded clay aggregates. L) Detail of Type 2 pedorelicts composing differentiated groundmass patches. Like in the overlying strata, these are loosely packed, partially welded, and bound by the same coating of highly birefringent chitonic illuvial clay.

of slackwater deposition with only seasonal spring discharge. Structured voids, weak aggregation, and laminated illuvial coatings point to prolonged ponding and percolation, with intermittent clay wetting and drying cycling. Such features are typical of a passive karst system, where slow epikarstic percolation and localised standing water dominate the sediment input, localized calcite precipitation, and the slow illuvial relocation of birefringent clays as observed trough the micromorphological and compositional analysis (Fig. 13C).

A renewed, stronger erosional phase is marked by erosional surfaces at the bottom of SU 39 (TD) and SU 24 (TB) with a localized phase of roof spall collapse at outer cave mouth. SU 24 shows a fining-upward trend with high TOC values and increased silt-clay content, reflecting decelerating floodwater and rapid sedimentation from sediment-laden flows. Micromorphological features, include laminated clay coatings, rounded charred plant remains, rolled Fe-Mn oxy-hydroxides nodules, and pedorelicts, and are indicative of short-lived, high-energy depositional events that reworked accumulated cave interior and epikarst sediments mixed with archaeological material. The archaeological assemblage suggests that these sediments were deposited during a phase of scattered human frequentation of the cave, with the surrounding landscape being more favoured for exploitation (Fig. 13D) (see e.g., Stoddart et al., 2019).

The uppermost preserved unit in the TD, SU 38a, shows a return to moderate sedimentation with seasonal ponds, as indicated by the identified ostracods, followed by a new erosional phase. The terminal middle Neolithic phase is characterized by SU 38a (TD) that correlates with SU 26 (TB). The absence of SU 25 in inner cave mouth is related to a channelled erosional event (Bronze Age phase, see next chapter). SU 26 and SU 25 are the best representations of the rhythmic sedimentation that characterizes the low-energy flood events at Grotta Battifratta cave. These events show well-defined fining-upward trends with sand-silt-clay laminae recognizable macroscopically, and further characterizable under the microscope as being, once again, composed of epikarst and endokarst reworked minerals and clay aggregates transported through the cave system to the outer cave mouth. Partial erosion of underlying archaeological strata and previously lain charcoal-rich sediments is responsible for the slight radiocarbon age inversion (SU 25; see Table 3) (Fig. 13E). During the deposition of SU 25 and SU 26, the cave was likely exploited only temporarily: the episodic flooding events that created the ephemeral ponds at the cave mouth, as also evidenced by the abundant ostracod assemblage, made it a strategic location for short-term access to fresh water. However, the same process made it unsuitable for stable occupation.

Overall, for the Middle Holocene, alternating low to moderate erosive inflows and depositional phases reflects not only changes in the biome of the external soil mantle on the slope, possibly even human-induced as a result of ancestral land management, but also episodic hydrological activation of the cave's passive drainage system, a pattern that is documented for other Holocene Apennine cave contexts (e.g. Tana della Mussina cave, Cremaschi et al., 2020, 2026). Clastic sediments were mobilised from the surrounding catchment during rainfall events capable of generating surface runoff and soil erosion and entered the cave through karst conduits and fractures. Under the microscope, these deposits consist mainly of soil aggregates (pedorelicts), Fe–Mn nodules, laminated coatings, and dispersed charcoal, pointing to the repeated mobilisation of pedogenetic material from charcoal-enriched cambisols and phaeozems developed outside the cave (see Napoli et al., 2019). These morphological and compositional signatures provide the sedimentary framework within which the Neolithic assemblage of pottery, lithic artifacts, and faunal remains was deposited, resulting in a palimpsest where cultural and natural components are closely intertwined, a process that is documented for several Neolithic cave sites in peninsular Italy, where slope wash and seasonal runoff, driven by warm and humid climate conditions often intensified by human-induced landscape disturbance, led to the rapid accumulation of fine sediments (see e.g., Boschian et al., 2017; Cremaschi et al., 2020; Rellini et al., 2020). These slope wash processes are consistent with broader palaeoecological evidence of increased fire activity, soil erosion, and vegetation disturbance since the middle Neolithic in central Italy. Charcoal and pollen records from sites such as Lago dell'Accesa indicate peaks in fire frequency around 7000 cal BP (Drescher-Schneider et al., 2007; Vannière et al., 2008), while multiple lake-pollen sequences reflect small-scale swidden agriculture and anthropogenic woodland clearance (Kelly and Huntley, 1991; Drescher-Schneider et al., 2007; Vannière et al., 2008; Stoddart et al., 2019). In our record, the presence of rounded brownish pedorelicts with a large amount of charred plant remains suggests a potential role of forest fires in destabilising slope soils, though we interpret these signals as indirect evidence of external firing episodes, rather than direct slash-and-burn activity at the site (see also Kelly and Huntley, 1991; Mercuri et al., 2002; Colombaroli et al., 2007; Vannière et al., 2008; Stoddart et al., 2019). During the Middle Neolithic (8000–6600 cal BP), central Italy underwent significant ecological changes driven by the interplay between climate variability and expanding human land-use (Mercuri et al., 2002; Vannière et al., 2008). Regional paleoclimate proxies indicate the climate was generally warm and humid, with occasional cooler and wetter oscillations (Stoddart et al., 2019 and reference therein). These conditions favoured the development of dense deciduous forests (*Quercus, Fagus, Carpinus*) and promoted stable soil formation processes on the surrounding slopes (Magri, 1999; Magri and Sadori, 1999; Mercuri et al., 2002; Guilizzoni et al., 2002; Drescher-Schneider et al., 2007; Sadori, 2018). Palaeoecological records from numerous lacustrine basins demonstrate an increasing anthropogenic footprint: the first appearances of *Triticum*, *Hordeum*, and *Cannabaceae* pollen precede or coincide with microcharcoal peaks and the rise of nitrophilous herbs (*Plantago*, *Urtica*), suggesting that fire was used deliberately to create and maintain open areas (Kelly and Huntley, 1991; Mercuri et al., 2002; Colombaroli et al., 2007; Vannière et al., 2008). This anthropogenic disturbance was

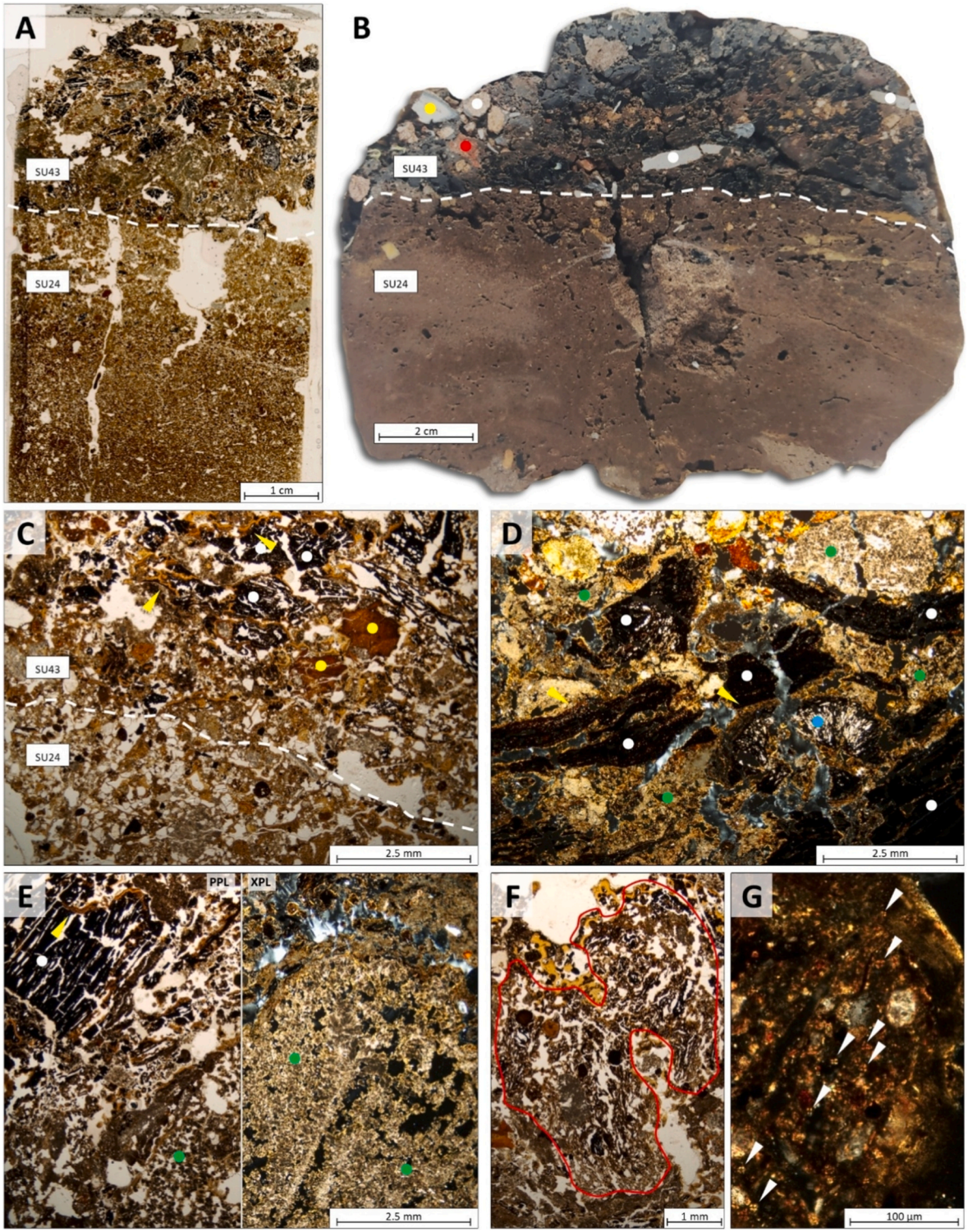


**Fig. 12.** Thin section scan and selected photomicrographs of the fireplace. (A) Scanned thin section. SU24 is the host substrate; SU43 is the fireplace. B) Photo of the sliced resin-consolidated block. Included within the burnt mass are several limestone plaques (white dots) alongside calcined bones (yellow dot) and rubified limestone (red dots). C-E) Plane polarized and cross polarized light (PPL/XPL) details of the feature's burnt inclusions, comprising large charcoal fragments (white dots), calcined bones (yellow dots), and recrystallized ash (green dots), occasionally sparry (blue dot in (D)). Convolute and laminated clay illuviation is common, wrapping and coating soil lumps and burnt inclusions (yellow arrows). F) PPL view of a lump of partially burnt dung, possibly used as fire starting fuel. G) XPL detail of faecal spherulites (white arrows) found in the dung, suggesting caprovine origin.

moderate and spatially limited, leading to a mosaic-like landscape composed of forest patches, cleared plots, and secondary grasslands that Stoddart et al. (2019) interpret, for its early phase, as one of "initial engagement" with the landscape, characterised by small-scale clearance within an otherwise forested matrix.

Comparable couplings between fire activity, accelerated hillslope erosion, and the expansion of agropastoral land use have also been reported in other European and eastern Mediterranean contexts. Several

**Table 3**
Radiocarbon dates from the TB and TD.

| Name sample | SU | Trench | Lab code | Age BP not calibrated | Material | 14C cal yr BP (2σ) IntCal20 | Reference timeframe for central Italy (after Palmisano et al., 2021) |
|---|---|---|---|---|---|---|---|
| GB 21 TB C2 US 25 | 25 | B | LTL22173 | 6177 ± 40 | Charcoal | 7167-6950 (94.3%) | Middle Neolithic (7150-6450 BP) 5200-4500 BC |
| GB 21 TB C3 US 24 | 24 | B | LTL22174 | 6153 ± 45 | Charcoal | 7165-6930 (93.5%) | Middle Neolithic (7150-6450 BP) 5200-4500 BC |
| GB22 US 45 TB Q11 | 45 | B | LTL31725 | 6184 ± 40 | Charcoal | 7167-6956 (92.8%) | Middle Neolithic (7150-6450 BP) 5200-4500 BC |
| GB 23 US 71 Adult human individual | Bottom 60 | B | LTL33852 | 6155 ± 40 | Bone | 7165-6940 (95,4%) | Middle Neolithic (7150-6450 BP) 5200-4500 BC |
| GB 21 US 43 | Combustion feature/SU 43- TOP SU 24 | B | LTL22170 | 3159 ± 35 | Charcoal | 3454-3332 (88.7%) | Middle Bronze Age (3650-3275/3250 BP/1700 1325/1300 BC) |
| GB 21 TD TOP US 37 | Top 37 | D | LTL22169 | 2954 ± 30 | Charcoal | 3210-3002 (95.4%) | Late/Final Bronze Age (LBA3275/3250-3100 BP/ 1325/1300-1150 BC) (FBA 3100-2950 BP/1150 -1000 BC) |
| GB 21 TD BOTTOM US 37 | Bottom 37 | D | LTL22175 | 3363 ± 45 | Charcoal | 3700-3465 (95.4%) | Middle Bronze Age (3650-3275/3250 BP//1700 1325/1300 BC) |
| GB 21 TD US 40 | 40 | D | LTL22171 | 6107 ± 40 | Charcoal | 7158-6882 (94.1%) | Middle Neolithic (7150-6450 BP) 5200-4500 BC |

well documented case studies link mid-Holocene increases in fire activity and soil erosion to human land use practices in the northern Apennines (Italy), the eastern, western and south eastern Iberian Peninsula (Spain, Portugal), and the French Pyrenees and Prealps (e.g., Maggi et al., 1997; Iriarte, 2009; Bal et al., 2010; Gil Romera et al., 2010; Vescovi et al., 2010; Rius et al., 2011; Compostella et al., 2013; Simonneau et al., 2013; Branch and Marini, 2014; Tallón Armada et al., 2014; Revelles et al., 2015; Walsh et al., 2019; Simões et al., 2020; Cremaschi et al., 2026), as well as in Greek catchments and eastern Adriatic karst settings (Croatia) (e.g., Van Andel et al., 1990; Karkanas, 2001; Farrand, 2003; Forenbaher et al., 2013; Lawson et al., 2013; Berger et al., 2016; Glais et al., 2017; Kaniewski et al., 2018; Dean et al., 2020; Rousseau et al., 2025; Smrkulj et al., 2025).

### *7.2. Cave deposit infill formation from the Late Holocene to the 16th century CE*

The Late Holocene depositional dynamics at Grotta Battifratta cave indicate a reorganisation of sedimentation patterns in response to shifts in hydrological characters and the influence of confined karst morphology.

In the inner cave mouth, this phase is marked by a well-defined erosional surface at the base of SU 37, where a U-shaped incision suggests the transit of an energetic flow capable of eroding and reworking previously deposited Neolithic sediment. Field observations indicate that this high-energy floodwater event was confined to a limited portion of the outer cave mouth sector, where it carved through SUs 25 and 26, exposing the top of SU 24 (Fig. 14A).

A radiocarbon date from bottom of SU 37, thus pertaining to the immediate infilling of the freshly carved channel, places this event in the Middle Bronze Age (3700–3465 cal yr BP; Table 3). After this erosional event, the inner-outer cave mouth interface was partially dammed by a roof collapse that temporarily impounded water and promoted localized ponding in the inner cave mouth, leaving, however, drier ground at the outer cave mouth (Conati Barbaro et al., 2024a). The archaeological record during this phase is limited to the outer cave mouth area and comprises scattered faunal remains, fragmentary ceramics, and the combustion feature dated to 3454–3332 cal yr BP. Establishing its function is complex because, although it contains abundant burnt material, it lacks an underlying rubified horizon typical of *in situ* fire production (Zerboni, 2011; Nicosia and Stoops, 2017; Marras et al., 2026). However, its roughly circular plan and stratified infill of burnt layers and ash lenses still point to a structured combustion-related deposit. Rather than excluding a combustion-related origin, this lack may reflect limited preservation of the original hearth microstratigraphy, as similar cave and rock shelter contexts show that fire residues affected by cleaning, rake-out, dumping, trampling, or slight reworking may lose the typical structure of intact hearths while still preserving clear evidence of burning (Miller et al., 2010; Karkanas et al., 2015; Whitau et al., 2018; Marcazzan et al., 2022). Regardless of its exact nature, however, the feature contains a variety of components that complement the macroscopic faunal and ceramic remains recovered during excavation, further indicating cave use by the local Bronze Age community. Crucially, the occurrence within the burnt matter of faecal spherulites suggests the possibility of a pastoral component to cave use during this phase (Portillo et al., 2017, 2020).

The absence of reworking and shifting of the coarse biogenic inclusions implies that the archaeological layers were buried and sealed soon after formation, preserving their original layout and internal structure (Fig. 14B).

The infilling of SU 37, in the inner cave mouth sector, continued until the Late Bronze Age (3210–3002 cal yr BP; Table 3). Sedimentation during this phase was dominated by the formation of the fine micrite mud, deposited under low-energy conditions linked to limited runoff, slow percolation, and prolonged water stagnation behind the dammed area with abundant microfossils. Deposition was favoured by the low ventilation settings and humid micro-environment within the inner cave mouth, favourable to the formation of spring tufa (*sensu* Capezzuoli et al., 2014) (Fig. 14B). This phase, characterized by a reduced waterflow, may have been associated with a surface arrangement in the outer cave mouth, consisting of large ceramic sherds and flat stones designed to facilitate the outflow of water, and stratigraphically overlying the combustion feature below.

This local phase of reduced hydrological activity seems to contrast with broader regional trends, as by the Middle and Late Bronze Age (after ~4000 cal yr BP), central Italy experienced increasing climatic instability, marked by episodes of reduced precipitation, heightened fire activity, and expanding land use. Indeed, multiproxy palaeoecological records from pollen-lake sequences consistently indicate widespread deforestation, the spread of cereal cultivation, and the appearance of orchard species (*Olea, Vitis, Juglans*), alongside declining forest cover and rising sediment mobility (see also Kelly and Huntley, 1991; Drescher-Schneider et al., 2007; Mercuri et al., 2002, 2010; Sadori, 2018; Stoddart et al., 2019). Bioarchaeological data from Pastena cave, suggest the application of artificial management techniques to cultivated plants, such as legumes, during the Middle-Bronze Age (Cortese et al., 2022). These environmental and land-use dynamics reflect broader settlement dynamics, characterised by more nucleated habitation patterns and intensified exploitation of arable lowlands, often associated with erosion-prone land-use strategies on adjacent slopes (Ricci Lucchi et al.,

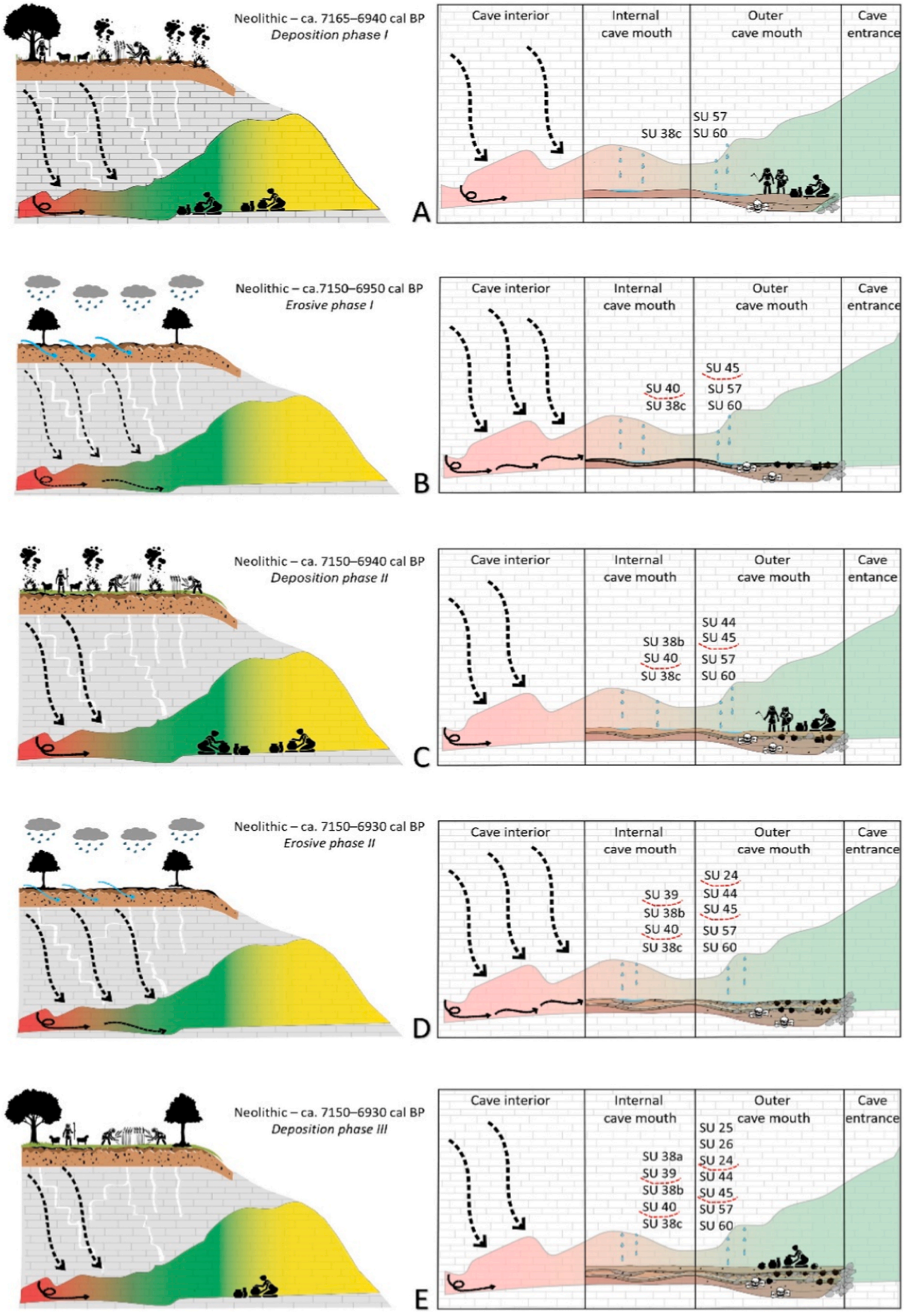


(caption on next page)

**Fig. 13.** Theoretical sketches showing the paleoclimatic and paleoenvironmental conditions during the Neolithic at Grotta Battifratta cave (ca. 7165–6930 cal BP), where it is highlighted the strong interaction between slope erosion, cave hydrology, and human activity. The succession begins with colluvial inputs of charcoal-rich soils derived from forested slopes, funnelled into the cave during warm, humid Early Holocene conditions (A). This stable phase is interrupted by the first erosive phase, when vegetation clearance triggered surface runoff and sediment reworking inside the cave (B). As slope dynamics stabilised, drip water-fed infiltration led to the quiet accumulation of fine, laminated silts in ponded, low-energy cave settings (C). A second erosive phase followed, likely linked to fire disturbance on the slopes, introducing charcoal, burnt bone, and disturbed soil aggregates into the cave system (D). In the final stage, previously deposited anthropogenic-rich sediments were internally remobilised by moderate flow events, forming layered silty-clay successions that mark the end of Neolithic infilling (E). Red dashed lines indicate erosional contacts; black arrows show the intensity of internal water flow; blue arrows depict slope runoff and infiltration into the karst system, and the skull with the bones represents the two different burials.

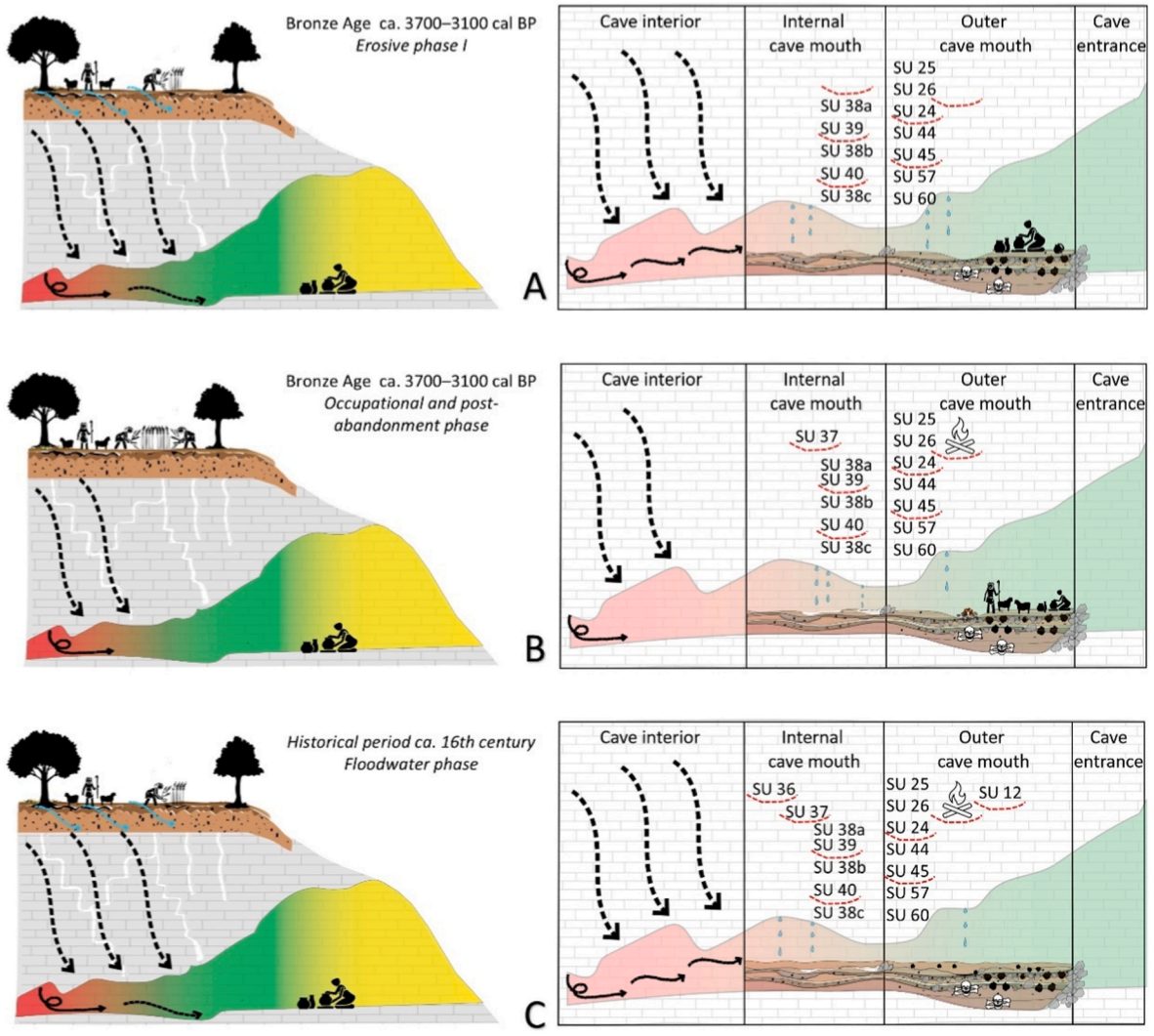


**Fig. 14.** Theoretical sketches illustrating the succession of depositional and erosional phases at Grotta Battifratta cave from the Bronze Age to the historical period, integrating evidence from both the external slope system and the internal cave environment. A Bronze Age erosive phase is marked by lateral incision into underlying Neolithic deposits (A). This is followed by short-term use of the cave, evidenced by a Middle Bronze Age hearth (3454–3332 cal BP) and by the accumulation of pf spring tufa (B). Finally, laminated, ash-rich, poorly sorted colluvial sediments (SU 12 – TB; SU 36 – TD) record a flood event during the 16th century CE, associated with the early phase of the Little Ice Age (C).

2000; Stoddart et al., 2019).

Subsequently, no further major depositional event is documented until the post-Medieval period. Around the 16$^{th}$ century CE, one or more high-energy floods reshaped the cave's morpho-sedimentary configuration, especially at the inner-outer cave mouth interface (Fig. 14C). This event is recorded as SU 12 (TB) and SU 36 (TD). Macroscopically, these are thick chaotic layers composed of variously laminated sediments alternating with coarse grain-size constituted by large, brecciated fragments of local travertine. Micromorphology reveals the presence of reworked and welded cave and epikarst clay deposits alongside ripped-up biogenic and anthropogenic inclusions from the older layers. Crucially, the finding of 16$^{th}$ century CE ceramic fragments (Fig. 5G), aligns this chaotic sediment input with pulses belonging to a broader phase of hydroclimatic instability observed across central and northern Italy during the early stages of the Little Ice Age (LIA), a period of intense cooling that triggered geomorphic processes and prompted anthropic land management responses that occurred between roughly AD 1300 and 1850 (Mann, 2002; Grove, 2019; Brandolini et al., 2025). Regional paleoenvironmental and historical records, particularly from lake sediment core of the Rieti Basin ~40 km north, attest to heightened rainfall, frequent flooding, and extensive slope destabilisation between the mid-15$^{th}$ and early 17$^{th}$ centuries CE (Mensing et al., 2018).

Multiproxy data from this period reveal increased erosion indicators in the lake (e.g. titanium and *Glomus* spores) and expanded waterlogged environments (*Alnus* pollen), pointing to enhanced geomorphic instability and wetted winters across the Mediterranean (Mensing et al., 2016, 2018). According to historical sources, the 16$^{th}$ century saw frequent flooding in Rome, with particularly severe events in 1530, when the Tiber reached 18.95 m at Ripetta (Rome city centre), and in December 1598, which remains the highest historical flood at 19.56 m (Bencivenga and Bersani, 2014).

## 8. Conclusions

The geoarchaeological investigation of the cave deposits of Grotta Battifratta provides new insights into central Italian Holocene climate changes, recorded as an interplay between karst hydrology, soil availability, local biome and human activity. Sediment inputs derived from slope erosion, episodic inflow, and carbonate precipitation were repeatedly reworked, creating a composite stratigraphy in which archaeological assemblages are recorded within deposits of mixed natural and anthropogenic origin. The archaeological record is therefore best interpreted as a palimpsest shaped by alternating depositional, erosional, and post-depositional processes.

During the Neolithic, generally warm and humid conditions supported dense forests, but the evidence for soil erosion and surface fire, emerged in the form of inherited brown soil pedorelicts and transported charcoal, may support the hypothesis that forest clearance was taking place to support agricultural or pastoral land use. This interpretation is consistent with continental scale syntheses and regional case studies showing that mid Holocene increases in fire activity and hillslope erosion often track the spread of agropastoral land use, where repeated clearance and burning were used to maintain open ground, extend cultivable and grazing areas, and in some settings to enhance soil productivity.

Placed within the wider archaeological and palaeoenvironmental framework of central Italy, the Grotta Battifratta sequence also supports a broader reassessment of Neolithic cave use. Inland sectors show a clear intensification of cave frequentation, particularly in connection with funerary practices (Grifoni Cremonesi, 2020, 2022). In this context, the classic Neolithic narrative focused on permanent villages and long-term settlement stability is less explanatory, and more dispersed settlement patterns and flexible strategies of land and resource use become more plausible (Robb, 2007; Stoddart et al., 2019). Consequently, cave assemblages are better interpreted not simply as a reflection of domestic occupation, but rather as the material outcome of practices with specific social and symbolic meanings that differ from those structured in open air settlements (Silvestri et al., 2020).

In the Bronze Age, the use of the cave became sporadic, possibly reflecting decreasing rainfall and the regional shift to nucleated lowland settlement locally known for this period. Erosional reworking and episodes of carbonate precipitation altered the cave's stratigraphic framework, demonstrating the sensitivity of karst environments to climatic and anthropogenic pressures. The final infilling during the early LIA reflects a sudden phase of flooding associated with intensified rainfall and slope instability, sealing the archive of earlier occupations.

Grotta Battifratta stands out as a multi-phase Holocene archive of local climate dynamics, in which cultural evidence acted intermittently as a conditioning factor in depositional processes. By framing its archaeological deposits within the wider context of karst hydrology and Holocene climate history, Grotta Battifratta contributes to a broader understanding of how societies and environments co-evolved in central Italy.

## Ethics statement

Excavation, sampling, and study of archaeological materials, including human remains, were authorised by the competent Italian heritage authorities (MiC) and carried out.

## CRediT author statement

All authors contributed substantially to the research presented here and to the paper, and they all approved the final version of the manuscript. In particular, the authors contributed to the following parts: Conceptualisation (LF, CCB), Methodology (LF, SC, DT, IM, PL, AP, AZ, CCB), Field investigation (LF, AM, ER, DM, ECa, ECh, MMu, NM, CCB), Formal analysis (LF, SC, DT ,IM, PL, AP, AZ, CCB), Writing – original draft (LF, SC, CCB), Writing – review and editing (LF, SC, SM, DT, IM, PL, ER, AM, DM, AZ, CCB), Visualisation (LF, SC, DT, CCB), Supervision (LF, SM, IM, AZ, CCB).

## Funding acknowledgements

The excavation of The excavation of Grotta Battifratta cave was carried out under concession from the Italian Ministry of Culture (MiC), DG-ABAP|28/04/2021|DECRETO 366; DG-ABAP|17/05/2023|DECRETO 631. The work was funded by Sapienza University of Rome, thanks to the Finanziamento Ricerche di Ateneo 2019 - Grandi Scavi 2021 [Grant no: SA12117A5EDC6DFD]; Grandi Scavi 2022 [Grant no: SA122181619BC153]; Grandi Scavi 2023 [Grant no: SA1231888CF265F7]; Grandi Scavi 2024 [Grant no: SA1241900E726869]. LF is supported by a research fellowship funded by the Italian Ministry of University and Research (MUR) through the project "Dipartimenti di Eccellenza 2023–2027″ awarded to the Dipartimento di Scienze della Terra "A. Desio" of the Università degli Studi di Milano (WP3). Additional financial support derived from the Cultural Heritage Active Innovation for Sustainable Society (CHANGES) Project, funded by the European Union – NextGenerationEU, under the National Recovery and Resilience Plan (NRRP) Mission 4 Component 2 Investment Line 1.3.

## Declaration of competing interest

The authors declare that they have no known competing financial interests or personal relationships that could have appeared to influence the work reported in this paper.

## Acknowledgements

We would like to thank Dr N. Fagiani, A. Betori, and F. Licordari, officials of the Soprintendenza Archeologia, Belle Arti e Paesaggio for the Metropolitan Area of Rome and the Province of Rieti, for their constant support over the years. We are also grateful to the Municipality of Poggio Nativo (Rieti prov.), as well as to both the former (V. Diamilla) and the current mayor (G. Vagni), for their valuable assistance. We thank Dr G. Filippi, Director of the Museo Civico di Salisano, for his helpful advice; Dr. C. Ranieri and the Gruppo Speleologico Vespertilio for their support in speleological activities; and the Associazione Sabina Cultura e Ambiente for their invaluable assistance. We are also grateful to Maurizio Trojano and the Associazione Cammini dell'Arte for their availability and logistical support. Special thanks are also due to all the students for their participation in the archaeological excavations.

## Appendix A. Supplementary data

Supplementary data to this article can be found online at https://doi.org/10.1016/j.quascirev.2026.110007.

## Data availability

All data and/or code is contained within the submission.

## References


Acanfora, M.O., 1962. Gli scavi di Valle Ottara presso Cittaducale. Bullettino di Paletnologia Italiana, n.s XIV (71–72), 73–154.

Albertini, D., Bassetti, M., Boccuccia, P., Bove, I., Di Gennaro, F., Di Lella, R.A., Marconi, N., Potì, A., 2019. Dalle scoperte alla valorizzazione in un'area dell'Appennino centrale. Progetto di studio, ricognizione e scavo nelle valli del Velino e del Salto a Cittaducale (RI). In: Rubat Borel, F. (Ed.), Preistoria E Protostoria in Ambiente Montano: Scoperte E Ricerca Territoriale, Tutela E Valorizzazione. Settimo Incontro Annuale Di Preistoria E Protostoria (7 Giugno 2019, Torino). Istituto Italiano di Preistoria e Protostoria, Torino, pp. 107–109.

Aldeias, V., Stahlschmidt, M.C., 2024. Sediment DNA can revolutionize archaeology—if it is used the right way. Proc. Natl. Acad. Sci. USA 121 (26), e2317042121. https://doi.org/10.1073/pnas.2317042121.

Angelucci, D.E., Arnaud, J., Zambaldi, M., Tessari, U., Vaccaro, C., Berruti, G.L.F., Daffara, S., Arzarello, M., 2019. New insights on the monte Fenera Palaeolithic, Italy: geoarchaeology of the Ciota Ciara cave. Geoarchaeology 34, 413–429. https://doi.org/10.1002/gea.21708.

Angelucci, D.E., Boschian, G., Fontanals, M., Pedrotti, A., Vergès, J.M., 2009. Shepherds and karst: the use of caves and rock-shelters in the Mediterranean region during the Neolithic. World Archaeol. 41 (2), 191–214. https://doi.org/10.1080/00438240902843659.

Bal, M.C., Rendu, C., Ruas, M.P., Campmajo, P., 2010. Paleosol charcoal: reconstructing vegetation history in relation to agro-pastoral activities since the Neolithic. A case study in the Eastern French pyrenees. J. Archaeol. Sci. 37, 1785–1797. https://doi.org/10.1016/j.jas.2010.01.035.

Bencivenga, M., Bersani, P., 2014. Influenza delle variazioni del clima sulle piene del Tevere a Roma. Mem. Descr. Carta Geol. Ital. XCVI, 377–386.

Berger, J.-F., Lespez, L., Kuzucuoğlu, C., Glais, A., Hourani, F., Barra, A., Guilaine, J., 2016. Interactions between climate change and human activities during the early to mid-Holocene in the eastern Mediterranean basins. Clim. Past 12 (9), 1847–1877. https://doi.org/10.5194/cp-12-1847-2016.

Biondi, E., Blasi, C., Allegrezza, M., Anzellotti, I., Azzella, M.M., Carli, E., et al., 2014. Plant communities of Italy: the Vegetation Prodrome. Plant Biosyst. 148 (4), 728–814. https://doi.org/10.1080/11263504.2014.948527.

Boomer, I., Horne, D.J., Slipper, I.J., 2003. The use of ostracods in palaeoenvironmental studies, or what can you do with an ostracod shell? Palaeontol. Soc. Pap. 9, 153–180. https://doi.org/10.1017/S1089332600002199.

Boschian, G., Martini, F., Sarti, L., 2017. Change fast or change slow? Late Glacial and Early Holocene cultures in a changing environment at Grotta Continenza, central Italy. Quat. Int. 450, 186–208. https://doi.org/10.1016/j.quaint.2016.12.027.

Bottacci, A., Clauser, F., 2022. INFC 2015. L'altra faccia della medaglia. L'Italia Forestale e Montana 77 (1), 49–54. https://doi.org/10.36253/ifm-1619.

Branch, N.P., Marini, N.A., 2014. Mid-Late Holocene environmental change and human activities in the northern Apennines, Italy. Quat. Int. 353, 34–51. https://doi.org/10.1016/j.quaint.2013.07.053.

Brandolini, F., Kinnaird, T.C., Srivastava, A., Costanzo, S., Compostella, C., Turner, S., 2025. Geoarchaeology reveals development of terrace farming in the Northern Apennines during the Medieval Climate Anomaly. Sci. Rep. 15, 24989.

Brown, A.G., 2013. Multi-proxy study of Holocene environmental change and human activity in the central Apennine Mountains, Italy. J. Quat. Sci. 28 (4), 380–394. https://doi.org/10.1002/jqs.2591.

Bulgarelli, G.M., 1979. Valle Ottara (Cittaducale, Prov. di Rieti), 34. Rivista di Scienze Preistoriche, pp. 320–321.

Canti, M.G., 1997. An investigation of microscopic calcareous spherulites from herbivore dungs. J. Archaeol. Sci. 24 (3), 219–231. https://doi.org/10.1006/jasc.1996.0105.

Capezzuoli, E., Gandin, A., Pedley, M., 2014. Decoding tufa and travertine (freshwater carbonates) in the sedimentary record: the state of the art. Sedimentology 61 (1), 1–21. https://doi.org/10.1111/sed.12075.

Carletti, E., Allegretta, I., Cardarelli, L., Forti, L., Monno, A., Terzano, R., Eramo, G., 2025a. Chert sources and territorial behaviour after the Neolithization process: an exploratory analysis from Grotta Battifratta (Rieti, Central Italy). Quat. Int. 717, 109633. https://doi.org/10.1016/j.quaint.2024.109633.

Carletti, E., Allegretta, I., Forti, L., Terzano, R., Eramo, G., 2026. Geochemical Data of Maiolica Chert from Central Italy for Provenance Studies. Journal of Open Archaeology Data 14, 7. https://doi.org/10.5334/joad.198. http://openarchaeologydata.metajnl.com/articles/10.5334/joad.198/.

Carletti, E., Eramo, G., Allegretta, I., Forti, L., Terzano, R., Conati Barbaro, C., 2025b. Geochemical data of Scaglia Bianca chert from Central Italy for provenance studies. J. Open Archaeol. Data 13 (8), 1–6. https://doi.org/10.5334/joad.155.

Carroll, D., 2012. Rock Weathering. Springer, Dordrecht. https://doi.org/10.1007/978-1-4684-1794-4.

Colombaroli, D., Marchetto, A., Tinner, W., 2007. Long-term interactions between Mediterranean climate, vegetation and fire regime at Lago di Massaciuccoli (Tuscany, Italy). J. Ecol. 95 (4), 755–770. https://doi.org/10.1111/j.1365-2745.2007.01240.x.

Compostella, C., Trombino, L., Caccianiga, M., 2013. Late Holocene soil evolution and treeline fluctuations in the Northern Apennines. Quat. Int. 289, 46–59. https://doi.org/10.1016/j.quaint.2012.02.011.

Conati Barbaro, C., Fiorucci, M., Grechi, G., Forti, L., Marmoni, G.M., Martino, S., 2024b. Safeguarding archaeological excavations and preserving cultural heritage in cave environments through engineering geological and geophysical approaches. J. Archaeolog. Sci.: Rep. 60, 104868. https://doi.org/10.1016/j.jasrep.2024.104868.

Conati Barbaro, C., Medeghini, L., Calzolari, L., Capriotti, S., Ciccola, A., 2025. La figurina fittile di Grotta Battifratta (Poggio Nativo, Rieti): una nuova rappresentazione antropomorfa del Neolitico dell'Italia Centrale, 2025. Rivista di scienze preistoriche: LXXV, pp. 1–14.

Conati Barbaro, C., Milli, S., Celant, A., Forti, L., Marconi, N., Moscone, D., Carletti, E., Chiarabba, E., Filippi, G., 2024a. La frequentazione pre-protostorica della Grotta Battifratta (Poggio Nativo, RI). Primi risultati di una nuova ricerca interdisciplinare. In: Lambusier, L., Ghini, G., Mari, Z. (Eds.), *Lazio and Sabina* 13. Quasar Edizioni, Roma, pp. 91–98.

Cortese, F., De Angelis, F., Achino, K.F., Bontempo, L., di Cicco, M.R., Gatta, M., Lubritto, C., Salari, L., Silvestri, L., Rickards, O., Rolfo, M.F., 2022. Isotopic reconstruction of the subsistence strategy for a Central Italian Bronze Age community (Pastena cave, 2nd millennium BCE). Archaeol. Anthropol. Sci. 14, 201. https://doi.org/10.1007/s12520-022-01673-5.

Cosentino, D., Cipollari, P., Marsili, P., Scrocca, D., 2010. Geology of the central Apennines: a regional review. J. Virtual Explor. 36 (11), 1–37. https://doi.org/10.3809/jvirtex.2010.00223.

Costanzo, S., Pappalardo, M., Starnini, E., Rossoni-Notter, E., Notter, O., Moussous, A., Zerboni, A., 2024. Integrating musealized archaeological sediment collections into current geoarchaeological analytical frameworks for sustainable research practices. MethodsX 13, 102897.

Cremaschi, M., Borgi, F., Malvini, M., 2020. Depositi alluvionali nei rami fossili della Tana della Mussina. Cambiamenti ambientali e frequentazione antropica nell'Olocene. In: Tirabassi, I., Formella, W., Cremaschi, M. (Eds.), La Tana Della Mussina Di Borzano. Dallo Scavo Pionieristico Dell'Ottocento Agli Studi Scientifici Del Ventunesimo Secolo. Università degli Studi di Milano, Milano, pp. 171–190.

Cremaschi, M., Ferraro, F., Peresani, M., Tagliacozzo, A., 2005. Il sito: nuovi contributi sulla stratigrafia, la cronologia, le faune a macromammiferi e le industrie del Paleolitico antico. In: Broglio, A., Dalmeri, G. (Eds.), Memorie Museo Civico Di Storia Naturale Di Verona, vol. 9. Museo delle Scienze, Italy, pp. 12–22.

Cremaschi, M., Nicosia, C., Favero, M., 2022. Extreme diagenesis in the Late Pleistocene stratigraphic sequence of Grotta Guattari (central Italy) and its impact on the archaeological record. Quat. Sci. Rev. 298, 107732. https://doi.org/10.1016/j.quascirev.2022.107732.

Cremaschi, M., Regattieri, E., Zanchetta, G., Isola, I., Hellstrom, J.C., Zerboni, A., 2026. Karst record of Holocene climate and human-induced changes in surface processes in the northern Apennines of Italy. Catena 266, 109960. https://doi.org/10.1016/j.catena.2026.109960.

Cremaschi, M., Zerboni, A., Mercuri, A.M., Olmi, L., Biagetti, S., Di Lernia, S., 2014. Takarkori rock shelter (SW Libya): an archive of Holocene climate and environmental changes in the central Sahara. Quat. Sci. Rev. 101, 36–60. https://doi.org/10.1016/j.quascirev.2014.07.004.

Cremaschi, M., Ferraro, F., 2007. The upper Pleistocene in the Paglicci Cave (Gargano, southern Italy): loess and tephra in the anthropogenic sequence. Atti Soc. Tosc. Sci. Nat., Mem., Ser. A 153–163.

De Waele, J., Gutiérrez, F., 2022. Karst Hydrogeology, Geomorphology and Caves. John Wiley and Sons, Chichester. https://doi.org/10.1002/9781119605379.

Dean, S., Pappalardo, M., Boschian, G., Spada, G., Forenbaher, S., Juračić, M., Miracle, P. T., 2020. Human adaptation to changing coastal landscapes in the Eastern Adriatic: evidence from Vela Spila cave, Croatia. Quat. Sci. Rev. 244, 106503. https://doi.org/10.1016/j.quascirev.2020.106503.

Degen, T., Sadki, M., Bron, E., König, U., Nénert, G., 2014. The HighScore suite. Powder Diffr. 29 (S2), S13–S18. https://doi.org/10.1017/S0885715614000840.

Drescher-Schneider, R., de Beaulieu, J.-L., Magny, M., Walter-Simonnet, A.-V., Bossuet, G., Millet, L., Brugiapaglia, E., Drescher, A., 2007. Vegetation history, climate and human impact over the last 15,000 years at Lago dell'Accesa (Tuscany, Central Italy). Veg. Hist. Archaeobot. 16 (4), 279–299. https://doi.org/10.1007/s00334-006-0089-z.

Eshel, G., Levy, G.J., Mingelgrin, U., Singer, M.J., 2004. Critical evaluation of the use of laser diffraction for particle-size distribution analysis. Soil Sci. Soc. Am. J. 68 (3), 736–743. https://doi.org/10.2136/sssaj2004.7360.

Farrand, W.R., 2001. Sediments and stratigraphy in rockshelters and caves: a personal perspective on principles and pragmatics. Geoarchaeology 16 (5), 537–557. https://doi.org/10.1002/gea.1004.

Farrand, W.R., 2003. Depositional environments and site formation during the Mesolithic occupations of Franchthi Cave, Peloponnesos, Greece. In: Galanidou, N., Perlès, C. (Eds.), *The Greek Mesolithic: Problems and Perspectives* (Brit. Sch. Athens Stud. 10). British School at Athens, London, pp. 69–78.

Filippi, G., Pacciarelli, M., 1991. Materiali protostorici dalla Sabina tiberina. In: Quaderni Del Museo Civico Di Rieti, vol. 1.

Ford, D., Williams, P.D., 2007. Karst Hydrogeology and Geomorphology. John Wiley and Sons, Chichester. https://doi.org/10.1002/9781118684986.

Forenbaher, S., Kaiser, T., Miracle, P.T., 2013. Dating the east Adriatic Neolithic. Eur. J. Archaeol. 16 (4), 589–609. https://doi.org/10.1179/1461957113Y.0000000038.

Ghinassi, M., Colonese, A.C., Di Giuseppe, Z., Govoni, L., Lo Vetro, D., Malavasi, G., Sala, B., 2009. The Late Pleistocene clastic deposits in the Romito Cave, southern Italy: a proxy record of environmental changes and human presence. J. Quat. Sci. 24 (4), 383–398. https://doi.org/10.1002/jqs.1236.

Gil-Romera, G., Carrión, J.S., Pausas, J.G., Sevilla-Callejo, M., Lamb, H.F., Fernández, S., Burjachs, F., 2010. Holocene fire activity and vegetation response in South-Eastern Iberia. Quat. Sci. Rev. 29 (9–10), 1082–1092. https://doi.org/10.1016/j.quascirev.2010.01.006.

Glais, A., Lespez, L., Vannière, B., López-Sáez, J.A., 2017. Human-shaped landscape history in NE Greece. A palaeoenvironmental perspective. J. Archaeol. Sci. Rep. 15, 405–422. https://doi.org/10.1016/j.jasrep.2017.06.017.

Goldberg, P., Sherwood, S.C., 2006. Deciphering human prehistory through the geoarchaeological study of cave sediments. Evol. Anthropol. 15 (1), 20–36. https://doi.org/10.1002/evan.20094.

Grifoni Cremonesi, R., 2020. Grotte, fosse, circoli di pietre, offerte vegetali e animali, acque e simboli: testimonianze di culti e riti nella preistoria italiana. Atti Soc. Tosc. Sci. Nat., Mem., Ser. A 127, 15–28.
Grifoni Cremonesi, R., 2022. L'uso delle cavità naturali in funzione domestica e/o cultuale: alcuni esempi dalla preistoria italiana. Preistoria Protost. Etruria (PPE) XV, 21–41.
Grove, J.M., 2019. The Little Ice Age. Routledge, London.
Guidi, A., Santoro, P., 2012. La preistoria e la protostoria in Sabina. In: L'Etruria Dal Paleolitico Al Primo Ferro. Lo Stato Delle Ricerche, Preistoria E Protostoria in Etruria, vol. 10, pp. 619–634.
Guilizzoni, P., Lami, A., Marchetto, A., Jones, V., Manca, M., Bettinetti, R., 2002. Palaeoproductivity and environmental changes during the Holocene in central Italy as recorded in two crater lakes (Albano and Nemi). Quat. Int. 88 (1), 57–68. https://doi.org/10.1016/S1040-6182(01)00073-8.
Hall, K., Thorn, C., Sumner, P., 2012. On the persistence of 'weathering'. Geomorphology 149, 1–10. https://doi.org/10.1016/j.geomorph.2011.12.024.
Hunt, C.O., Gilbertson, D.D., Hill, E.A., Simpson, D., 2015. Sedimentation, re-sedimentation and chronologies in archaeologically important caves: problems and prospects. J. Archaeol. Sci. 56, 109–116. https://doi.org/10.1016/j.jas.2015.02.030.
Iaconis, M.A., Boschian, G., 2008. Geoarchaeology of the deposits of Grotta dei Piccioni and Grotta Sant'Angelo (Abruzzo, Central Italy). Atti Soc. Tosc. Sci. Nat. 112, 181–188.
Ingersoll, R.V., Bullard, T.F., Ford, R.L., Grimm, J.P., Pickle, J.D., Sares, S.W., 1984. The effect of grain size on detrital modes: a test of the Gazzi–Dickinson point-counting method. J. Sediment. Res. 54, 103–116. https://doi.org/10.1306/212F83B9-2B24-11D7-8648000102C1865D.
Iriarte, M.J., 2009. Vegetation landscape and the anthropization of the environment in the central sector of the Northern Iberian Peninsula: current status. Quat. Int. 200, 66–76. https://doi.org/10.1016/j.quaint.2008.10.008.
ISPRA, 2022. *I Normali Climatici 1991–2020 Di Temperatura E Precipitazione in Italia.* Rapporto ISPRA/Stato Dell'Ambiente 99/2022. ISPRA, Roma.
Kaniewski, D., Marriner, N., Morhange, C., Rius, D., Carré, M.B., Faivre, S., Van Campo, E., 2018. Croatia's mid-late Holocene (5200–3200 BP) coastal vegetation shaped by human societies. Quat. Sci. Rev. 200, 334–350. https://doi.org/10.1016/j.quascirev.2018.10.004.
Karkanas, P., 2001. Site formation processes in Theopetra Cave: a record of climatic change during the Late Pleistocene and Early Holocene in Thessaly, Greece. Geoarchaeology 16, 373–399. https://doi.org/10.1002/gea.1009.
Karkanas, P., Brown, K.S., Fisher, E.C., Jacobs, Z., Marean, C.W., 2015. Interpreting human behavior from depositional rates and combustion features through the study of sedimentary microfacies at site Pinnacle Point 5-6, South Africa. J. Hum. Evol. 85, 1–21. https://doi.org/10.1016/j.jhevol.2015.04.006.
Karkanas, P., Marean, C., Bar-Matthews, M., Jacobs, Z., Fisher, E., Braun, K., 2021. Cave life histories of non-anthropogenic sediments help us understand associated archaeological contexts. Quat. Res. 99, 270–289. https://doi.org/10.1017/qua.2020.72.
Kelly, M.G., Huntley, B., 1991. An 11,000-year record of vegetation and environment from Lago di Martignano, Latium, Italy. J. Quat. Sci. 6, 209–224. https://doi.org/10.1002/jqs.3390060304.
Lawson, I.T., Tzedakis, P.C., Roucoux, K.H., Galanidou, N., 2013. The anthropogenic influence on wildfire regimes: charcoal records from the Holocene and Last Interglacial at Ioannina, Greece. J. Biogeogr. 40, 2324–2334. https://doi.org/10.1111/jbi.12164.
Macphail, R.I., Goldberg, P., 2018. Applied Soils and Micromorphology in Archaeology. Cambridge University Press, Cambridge.
Maggi, R., Starnini, E., Biagi, P., 1997. In: Bernabò Brea, L. (Ed.), Arene Candide: a Functional and Environmental Assessment of the Holocene Sequence Excavated. Il Calamo, Genova, pp. 1940–1950.
Magri, D., 1999. Late Quaternary vegetation history at Lagaccione near Lago di Bolsena (central Italy). Rev. Palaeobot. Palynol. 106, 171–208. https://doi.org/10.1016/S0034-6667(99)00006-8.
Magri, D., Sadori, L., 1999. Late Pleistocene and Holocene pollen stratigraphy at Lago di Vico, central Italy. Veg. Hist. Archaeobot. 8, 247–260. https://doi.org/10.1007/BF01291777.
Mallol, C., Goldberg, P., 2017. Cave and rock shelter sediments. In: Nicosia, C., Stoops, G. (Eds.), Archaeological Soil and Sediment Micromorphology. Wiley, Chichester, pp. 359–381. https://doi.org/10.1002/9781118941065.ch34.
Manfra, L., Masi, U., Turi, B., 1976. La composizione isotopica dei travertini del Lazio. Geol. Rom. 15, 127–174.
Mann, M.E., 2002. Little ice Age. In: Encyclopedia of Global Environmental Change, vol. 1. Wiley, Chichester, pp. 504–509.
Marcazzan, D., Miller, C.E., Conard, N.J., 2022. Burning, dumping, and site use during the Middle and Upper Palaeolithic at Hohle Fels Cave, SW Germany. Arch. and Anth. Sci. 14 (9). https://doi.org/10.1007/s12520-022-01647-7.
Marras, G.B., Marzullo, M., Schmidt, F., French, C., Sheldrake, M., Motta, L., et al., 2026. Beneath the city: micromorphological insights into Etruscan urban life, infrastructure, and ritual spaces from Tarquinia, Central Italy. Arch. and Anth. Sci. 18 (1), 3.
Massilani, D., Morley, M.W., Mentzer, S.M., Aldeias, V., Vernot, B., Miller, C., Meyer, M., 2022. Microstratigraphic preservation of ancient faunal and hominin DNA in Pleistocene cave sediments. Proc. Natl. Acad. Sci. USA 119, e2113666118. https://doi.org/10.1073/pnas.2113666118.
Mensing, S.A., Schoolman, E.M., Tunno, I., Noble, P.J., Sagnotti, L., Florindo, F., Piovesan, G., 2018. Historical ecology reveals landscape transformation coincident with cultural development in central Italy since the Roman period. Sci. Rep. 8, 2138. https://doi.org/10.1038/s41598-018-20286-4.
Mensing, S.A., Tunno, I., Cifani, G., Passigli, S., Noble, P., Archer, C., Piovesan, G., 2016. Human and climatically induced environmental change in the Mediterranean during the Medieval Climate Anomaly and Little Ice Age: a case from central Italy. Anthropocene 15, 49–59. https://doi.org/10.1016/j.ancene.2016.01.003.
Mercuri, A.M., Accorsi, C.A., Bandini Mazzanti, M., 2002. The long history of Cannabis and its cultivation by the Romans in central Italy, shown by pollen records from Lago Albano and Lago di Nemi. Veg. Hist. Archaeobot. 11, 263–276. https://doi.org/10.1007/s003340200039.
Mercuri, A.M., Sadori, L., Blasi, C., 2010. Editorial: archaeobotany for cultural landscape and human impact reconstructions. Plant Biosyst. 144, 860–864. https://doi.org/10.1080/11263504.2010.514137.
Miller, C.E., Conard, N.J., Goldberg, P., Berna, F., 2010. Dumping, sweeping and trampling experimental micromorphological analysis of anthropogenically modified combustion features. Palethnologie. Archéologie et sciences humaines (2). https://doi.org/10.4000/palethnologie.8197.
Morley, M.W., Moffat, I., Kotarba-Morley, A.M., Hernandez, V.C., Zerboni, A., Herries, A. I., Westaway, K., 2023. Why the geosciences are becoming increasingly vital to the interpretation of the human evolutionary record. Nat. Ecol. Evol. 7, 1971–1977. https://doi.org/10.1038/s41559-023-02215-5.
Moroni, A., Boschian, G., Crezzini, J., Montanari-Canini, G., Marciani, G., Capecchi, G., Spagnolo, V., 2019. Late Neandertals in central Italy: high-resolution chronicles from Grotta dei Santi (Monte Argentario–Tuscany). Quat. Sci. Rev. 217, 130–151. https://doi.org/10.1016/j.quascirev.2018.11.021.
Munsell Color Company, 1994. Munsell soil color charts. In: Macbeth Division of Kollmorgen, New Windsor, NY, Revised ed.
Murphy, C.P., 1986. Thin Section Preparation of Soils and Sediments. AB Academic Publishers, Berkhamsted.
Napoli, R., Paolanti, M., Di Ferdinando, S. (Eds.), 2019. Atlante Dei Suoli Del Lazio. ARSIAL Regione Lazio, Roma.
Nicosia, C., Stoops, G. (Eds.), 2017. Archaeological Soil and Sediment Micromorphology. Wiley, Chichester. https://doi.org/10.1002/9781118941065.
Palmisano, A., Bevan, A., Kabelindde, A., Roberts, N., Shennan, S., 2021. Long-term demographic trends in prehistoric Italy: climate impacts and regionalised socio-ecological trajectories. J. World Prehist. 34, 381–432. https://doi.org/10.1007/s10963-021-09159-3.
Pieruccini, P., Forti, L., Mecozzi, B., et al., 2022. Stratigraphic reassessment of Grotta Romanelli sheds light on middle–late Pleistocene palaeoenvironments and human settling in the Mediterranean. Sci. Rep. 12, 13530. https://doi.org/10.1038/s41598-022-16906-9.
Portillo, M., Belarte, M.C., Ramon, J., Kallala, N., Sanmartí, J., Albert, R.M., 2017. An ethnoarchaeological study of livestock dung fuels from cooking installations in northern Tunisia. Quat. Inter. 431, 131–144. https://doi.org/10.1016/j.quaint.2015.12.040.
Portillo, M., García-Suárez, A., Matthews, W., 2020. Livestock faecal indicators for animal management, penning, foddering and dung use in early agricultural built environments in the Konya Plain. Central Anatolia. Arch. and Anthr. Sci. 12 (2), 40. https://doi.org/10.1007/s12520-019-00988-0.
Reimer, P.J., Austin, W.E., Bard, E., Bayliss, A., Blackwell, P.G., Ramsey, C.B., Talamo, S., 2020. The IntCal20 Northern Hemisphere radiocarbon age calibration curve (0–55 cal kBP). Radiocarbon 62, 725–757. https://doi.org/10.1017/RDC.2020.41.
Rellini, I., Firpo, M., Isetti, E., Rossi, G., Robb, J., Pian, D., Traverso, A., 2020. Micromorphological investigations at Scaloria Cave (Puglia, south-east Italy): new evidence of multifunctional use of the space during the Neolithic. Archaeol. Anthropol. Sci. 12, 28. https://doi.org/10.1007/s12520-019-01005-0.
Rellini, I., Firpo, M., Martino, G., Riel-Salvatore, J., Maggi, R., 2013. Climate and environmental changes recognized by micromorphology in Palaeolithic deposits at Arene Candide (Liguria, Italy). Quat. Int. 315, 42–55. https://doi.org/10.1016/j.quaint.2013.05.050.
Revelles, J., Cho, S., Iriarte, E., Burjachs, F., van Geel, B., Palomo, A., Piqué, R., Peña-Chocarro, L., Terradas, X., 2015. Mid-Holocene vegetation history and Neolithic land-use in the Lake Banyoles area (Girona, Spain). Palaeogeogr. Palaeoclimatol. Palaeoecol. 435, 70–85. https://doi.org/10.1016/j.palaeo.2015.06.002.
Ricci Lucchi, M., Calderoni, G., Carrara, C., Cipriani, N., Esu, D., Ferreli, L., Nebbiai, M., 2000. Late Quaternary record of the Rieti Basin, central Italy: palaeoenvironmental and palaeoclimatic evolution. G. Geol. (Bologna) 62, 105–136.
Rius, D., Vannière, B., Galop, D., Richard, H., 2011. Holocene fire regime changes from multiple-site sedimentary charcoal analyses in the Lourdes basin (Pyrenees, France). Quat. Sci. Rev. 30, 1696–1709. https://doi.org/10.1016/j.quascirev.2011.03.014.
Robb, J., 2007. The Early Mediterranean Village: Agency, Material Culture, and Social Change in Neolithic Italy. Cambridge University Press, Cambridge. https://doi.org/10.1017/CBO9780511499647.
Rolfo, M.F., Achino, K.F., Fusco, I., Salari, L., Silvestri, L., 2016. Reassessing human occupation patterns in the inner central Apennines in prehistory: the case-study of Grotta Mora Cavorso. JAS Reports 7, 358–367.
Rousseau, M., Sorrel, P., Dièthre, B., Čaušević-Bully, M., Richard, H., 2025. Vegetation changes and human activities since the Bronze Age (late Holocene) in a coastal doline of the Kvarner archipelago (Croatia). Rev. Palaeobot. Palynol., 105483
Ryan, D.D., Starnini, E., Serradimigni, M., Rossoni-Notter, E., Notter, O., Zerboni, A., et al., 2024. A geoarchaeological review of Balzi Rossi, Italy: a crossroad of Palaeolithic populations in the northwest Mediterranean. Quat. Sci. Rev. 327, 108515. https://doi.org/10.1016/j.quascirev.2024.108515.
Sadori, L., 2018. The Lateglacial and Holocene vegetation and climate history of Lago di Mezzano (central Italy). Quat. Sci. Rev. 202, 30–44. https://doi.org/10.1016/j.quascirev.2018.09.004.

Sasowsky, I.D., Mylroie, J. (Eds.), 2007. Studies of Cave Sediments: Physical and Chemical Records of Paleoclimate. Springer, Berlin. https://doi.org/10.1007/978-1-4020-5766-3.

Segre Naldini, E., Biddittu, I., 1985. Ceramica dell'età del Bronzo dal Costone di Battifratta (Rieti). Archeol. Laziale VII, Quad. AEI 11, 26–33.

Segre Naldini, E., Biddittu, I., 1988. Ceramica neolitica dalle Grotticelle del Costone di Battifratta (Rieti). Archeol. Laziale IX, Quad. AEI 16, 369–371.

Geologico d'Italia, Servizio, 2009. *Carta geologica D'Italia* Alla Scala 1:50.000, Foglio 357 Cittaducale. ISPRA, Roma. https://doi.org/10.15161/oar.it/a15wc-rg802.

Silvestri, L., Achino, K.F., Gatta, M., Rolfo, M.F., Salari, L., 2020. Grotta Mora Cavorso: physical, material and symbolic boundaries of life and death practices in a Neolithic cave of central Italy. Quat. Int. 539, 29–38. https://doi.org/10.1016/j.quaint.2018.09.050.

Simões, C.D., Carvalho, A.F., Tente, C., 2020. "Neolithic geoarchaeology at Penedo dos Mouros Rockshelter: mid-holocene site formation, diagenesis and human activity at the foothills of Serra da Estrela (Portugal). Geoarchaeology 35 (4), 503–521. https://doi.org/10.1002/gea.21785.

Simonneau, A., Doyen, E., Chapron, E., Millet, L., Vannière, B., Di Giovanni, C., Bossard, N., Tachikawa, K., Bard, E., Albéric, P., Desmet, M., Roux, G., Lajeunesse, P., Berger, J.-F., Arnaud, F., 2013. Holocene land-use evolution and associated soil erosion in the French Prealps inferred from Lake Paladru sediments and archaeological evidences. J. Archaeol. Sci. 40, 1636–1645. https://doi.org/10.1016/j.jas.2012.12.002.

Smrkulj, N., Miko, S., Razum, I., Hasan, O., Brunović, D., Ilijanić, N., Huang, J.-J.S., Ortler, M., Hus, P., Šparica Miko, M., 2025. Holocene paleoenvironmental changes recorded in the sediments of the karst Krka River estuary (eastern Adriatic coast, Croatia). Catena 251, 108811. https://doi.org/10.1016/j.catena.2025.108811.

Spinapolice, E.E., Zerboni, A., Meyer, M.C., et al., 2022. Back to Uluzzo—Archaeological, palaeoenvironmental and chronological context of the Mid–Upper Palaeolithic sequence at Uluzzo C Rock Shelter (Apulia, southern Italy). J. Quat. Sci. 37, 217–234. https://doi.org/10.1002/jqs.3349.

Stoddart, S., Woodbridge, J., Palmisano, A., Mercuri, A.M., Mensing, S.A., Colombaroli, D., Roberts, C.N., 2019. Tyrrhenian central Italy: holocene population and landscape ecology. Holocene 29, 761–775. https://doi.org/10.1177/0959683619826696.

Stoops, G., 2021. Guidelines for Analysis and Description of Soil and Regolith Thin Sections. Soil Science Society of America, Madison, WI. https://doi.org/10.1002/9780891189763.

Stoops, G., Marcelino, V., Mees, F. (Eds.), 2018. Interpretation of Micromorphological Features of Soils and Regoliths. Elsevier, Amsterdam. https://doi.org/10.1016/C2014-0-01728-5.

Tallón-Armada, R., Costa-Casais, M., Schellekens, J., Taboada Rodríguez, T., Vives-Ferrándiz Sánchez, J., Ferrer García, C., Abel Schaad, D., López-Sáez, J.A., Carrión Marco, Y., Martínez Cortizas, A.M., 2014. Holocene environmental change in Eastern Spain reconstructed through the multiproxy study of a pedo-sedimentary sequence from Les Alcusses (Valencia, Spain). J. Archaeol. Sci. 47, 22–38. https://doi.org/10.1016/j.jas.2014.03.023.

Tarquini, S., Isola, I., Favalli, M., Battistini, A., Dotta, G., 2023. TINITALY, a Digital Elevation Model of Italy with a 10 Meters Cell Size. Istituto Nazionale di Geofisica e Vulcanologia (INGV). https://doi.org/10.13127/tinitaly/1.1, Version 1.1.

Thompson, J.E., 2024. Osteological Report on the Human Remains from Grotta Battifratta. Internal Report (unpublished).

Thompson, M.L., Ukrainczyk, L., 2002. Micas. In: Dixon, J.B., Schulze, D.G. (Eds.), Soil Mineralogy with Environmental Applications, vol. 7. Soil Science Society of America, Madison, pp. 431–466.

Van Andel, T.H., Zangger, E., Demitrack, A., 1990. Land use and soil erosion in prehistoric and historical Greece. J. Field Archaeol. 17, 379–396. https://doi.org/10.2307/530002.

Vannière, B., Colombaroli, D., Chapron, E., Leroux, A., Tinner, W., Magny, M., 2008. Climate versus human-driven fire regimes in Mediterranean landscapes: the Holocene record of Lago dell'Accesa (Tuscany, Italy). Quat. Sci. Rev. 27, 1181–1196. https://doi.org/10.1016/j.quascirev.2008.02.011.

Vescovi, E., Ammann, B., Ravazzi, C., Tinner, W., 2010. A new Late-glacial and Holocene record of vegetation and fire history from Lago del Greppo, northern Apennines, Italy. Veg. Hist. Archaeobot. 19, 219–233. https://doi.org/10.1007/s00334-010-0243-5.

Vigliotti, L., Ariztegui, D., Guilizzoni, P., Lami, A., 2010. Reconstructing natural and human-induced environmental change in central Italy since the Late Pleistocene: the multi-proxy records from maar lakes Albano and Nemi. In: IAVCEI Spec. Publ. (Geol. Soc. Lond.). https://doi.org/10.1144/IAVCEI003.13.

Walsh, K., Berger, J.-F., Roberts, C.N., Vannière, B., Ghilardi, M., Brown, A.G., Woodbridge, J., Lespez, L., Estrany, J., Glais, A., Palmisano, A., Finné, M., Verstraeten, G., 2019. Holocene demographic fluctuations, climate and erosion in the Mediterranean: a meta data-analysis. Holocene 29, 864–885. https://doi.org/10.1177/0959683619826637.

Whatley, R.C., 1988. Patterns and rates of evolution among Mesozoic Ostracoda. In: Hanai, T., Ikeya, N., Ishizaki, K. (Eds.), Developments in Palaeontology and Stratigraphy, vol. 11. Elsevier, Amsterdam, pp. 1021–1040.

Whitau, R., Vannieuwenhuyse, D., Dotte-Sarout, E., Balme, J., O'Connor, S., 2018. Home is where the hearth is: anthracological and microstratigraphic analyses of Pleistocene and Holocene combustion features, Riwi Cave (Kimberley, Western Australia). J.of Arch. Met. and Th. 25 (3), 739–776. https://doi.org/10.1007/s10816-017-9354-y.

White, W.B., 1988. Geomorphology and Hydrology of Karst Terrains. Oxford University Press, New York.

Woodward, J.C., Goldberg, P., 2001. The sedimentary records in Mediterranean rockshelters and caves: archives of environmental change. Geoarchaeology 16, 327–354. https://doi.org/10.1002/gea.1007.

World Meteorological Organization (WMO), 2017. *WMO Guidelines on the Calculation of Climate Normals*. WMO-No. 1203. WMO, Geneva. ISBN: 978-92-63-11203-3.

WRB, 2015. World Reference Base for Soil Resources 2014, Update 2015. FAO, Rome.

Zerboni, A., 2011. Micromorphology reveals *in situ* Mesolithic living floors and archaeological features in multiphase sites in central Sudan. Geoarchaeology 26 (3), 365–391.

Zerboni, A., Villa, F., Wu, Y.-L., Solomon, T., Trentini, A., Rizzi, A., Cappitelli, F., Gallinaro, M., 2022. The sustainability of rock art: preservation and research. Sustainability 14, 6305. https://doi.org/10.3390/su14106305.